


FULL PAPER

Open Access



Seismic clusters and fluids diffusion: a lesson from the 2018 Molise (Southern Italy) earthquake sequence

Stefania Gentili^{1*} , Piero Brondi¹, Giuliana Rossi², Monica Sukan², Giuseppe Petrillo^{3,4,5}, Jiancang Zhuang³ and Stefano Campanella²

Abstract

The identification of seismic clusters is essential for many applications of statistical analysis and seismicity forecasting: uncertainties in cluster identification leads to uncertainties in results. However, there are several methods to identify clusters, and their results are not always compatible. We tested different approaches to analyze the clustering: a traditional window-based approach, a complex network-based technique (nearest neighbor—NN), and a novel approach based on fractal analysis. The case study is the increase in seismicity observed in Molise, Southern Italy, from April to November 2018. To analyze the seismicity in detail with the above-mentioned methods, an improved template-matching catalog was created. A stochastic declustering method based on the Epidemic Type Aftershock Sequence (ETAS) model was also applied to add probabilistic information. We explored how the significant discrepancies in these methods' results affect the result of NExt STRong Related Earthquake (NESTORE) algorithm—a method to forecast strong aftershocks during an ongoing cluster—previously successfully applied to the whole Italian territory. We performed a further analysis of the spatio-temporal pattern of seismicity in Molise, using the Principal Component Analysis (PCA), the ETAS algorithm, as well as other analyses, aimed at detecting possible migration and diffusion signals. We found a relative quiescence of several months between the main events of April and August, the tendency of the events to propagate upwards, and a migration of the seismicity consistent with a fluid-driven mechanism. We hypothesize that these features indicate the presence of fluids, which are also responsible for the long duration of the sequence and the discrepancies in cluster identification methods' results. Such results add to the other pieces of evidence of the importance of the fluid presence in controlling the seismicity in the Apennines. Moreover, this study highlights the importance of refined methods to identify clusters and encourages further detailed analyses when different methods supply very different results.

Keywords Seismic cluster identification, Template-matching, Machine-learning, Nearest neighbor method, Fractals, Stochastic declustering, ETAS, Principal Component Analysis, Relative quiescence, Fluid diffusion

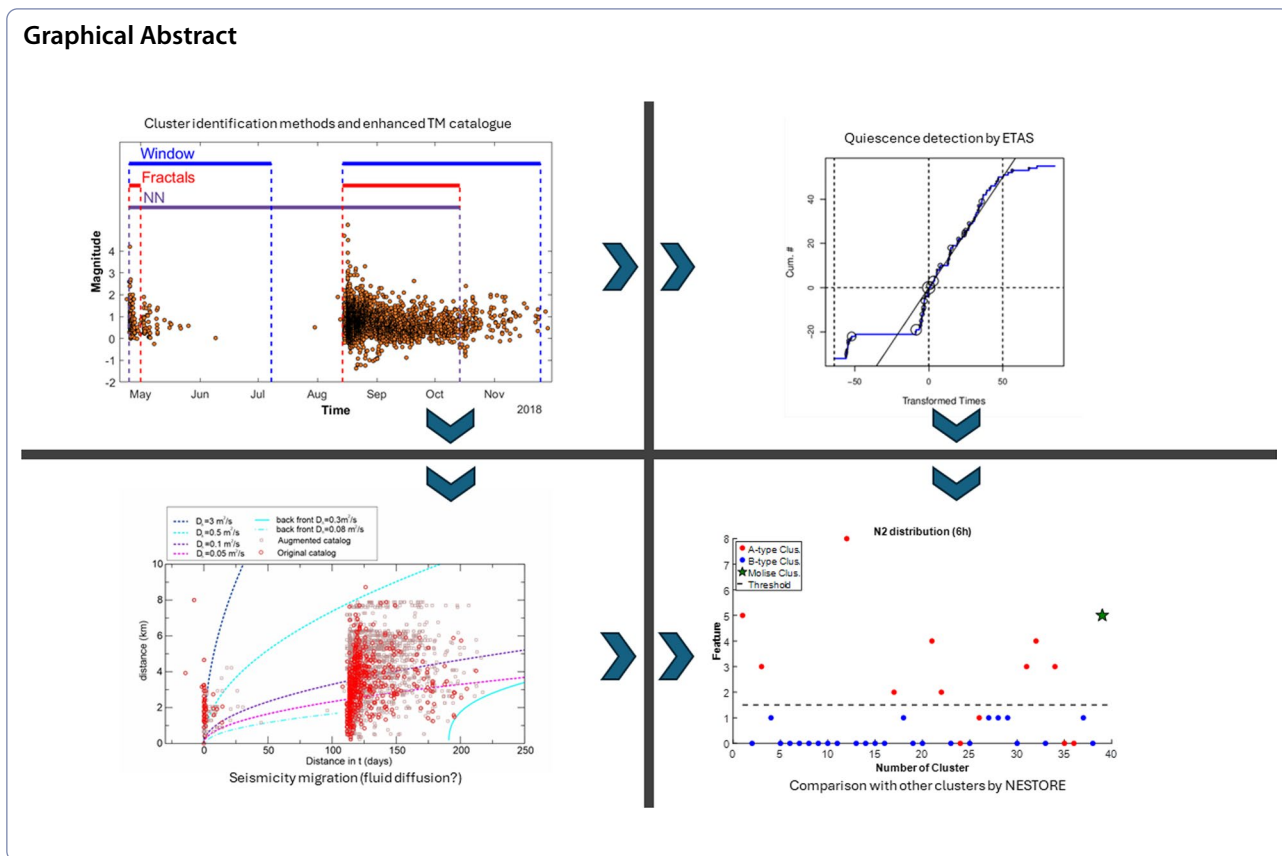
*Correspondence:

Stefania Gentili
sgentili@ogs.it

Full list of author information is available at the end of the article



© The Author(s) 2024. **Open Access** This article is licensed under a Creative Commons Attribution 4.0 International License, which permits use, sharing, adaptation, distribution and reproduction in any medium or format, as long as you give appropriate credit to the original author(s) and the source, provide a link to the Creative Commons licence, and indicate if changes were made. The images or other third party material in this article are included in the article's Creative Commons licence, unless indicated otherwise in a credit line to the material. If material is not included in the article's Creative Commons licence and your intended use is not permitted by statutory regulation or exceeds the permitted use, you will need to obtain permission directly from the copyright holder. To view a copy of this licence, visit <http://creativecommons.org/licenses/by/4.0/>.



1 Introduction

Human observation typically categorizes the seismic events based on their relative magnitudes and positions in the space–time sequence, identifying sequences and the so-called swarms. Earthquake sequences are associated with a mainshock, which is followed by smaller events nearby (Omori 1894; Gutenberg and Richter 1941; Kagan 1994; Turcotte 1997; Scholz 2002; Bak et al. 2002). Occasionally, the mainshock is preceded by small precursory events (Brodsky and Lay 2014; Mignan 2014; Seif et al. 2019; Petrillo and Lippiello 2021, 2023). However, seismic events can also form clusters known as swarms, where seismic activity is not distinctly tied to a mainshock, significantly larger than the others (Mogi 1963; 1989). A quantitative definition of swarm can be found in Mogi (1963). However, in recent times different quantitative definitions have been proposed (e.g., Hainzl and Fischer 2002). The identification of the seismic clusters is of paramount importance for statistical seismology. In fact, various statistical tests concerning relevant aspects of seismology, such as seismic hazard analysis and earthquake forecasting are carried out, assuming a good knowledge of the clusters in the data (van Stiphout et al. 2012). Moreover, many forecasting techniques, as

e.g., Short Term Aftershock forecasting (STAI), are also based on learning seismicity patterns (Lippiello et al. 2019b; Gentili and Di Giovambattista 2017, 2020, 2022; Gentili et al. 2023; Anyfadi et al. 2023; Brondi et al. 2024). Therefore, the better the cluster knowledge, the better the learning and the forecasting performance.

Unfortunately, clusters are not precisely defined in seismology. Earthquakes that belong to a cluster occur close in time and space to the mainshock, but how close in time and space they should be to belong to a cluster is controversial. In the literature, there are several methods for defining clusters. While earthquakes that are close in time and space are often easily recognized by all methods as belonging to the same cluster, for others the distance in time or space makes the attribution more challenging. This can lead to different segmentations of each cluster into smaller subclusters that can be different when different cluster analysis techniques are used.

In this paper, we focus on an increase in seismic activity in Molise region (Southern Italy) from April to November 2018. The increased activity started with an event of magnitude Mw 4.3 on 25 April 2018, a series of aftershocks until 9 May, and continued with an extremely low seismicity until 11 August, when an intense activity restarted, culminating with the event of Mw 5.1 on 16

August. We firstly detected an atypical behavior in space, time and energy evolution of this cluster during the application of the NESTOREv1.0 program (Gentili et al. 2023) to the whole Italian territory (Bronzi et al. 2023, 2024). The software uses the Next STRONG Related Earthquake (NESTORE) algorithm (Gentili et al. 2023), a machine-learning algorithm for cluster classification, whose aim is to forecast the probability of a strong aftershock with a magnitude (M_a) greater or equal to the magnitude of the mainshock (M_m) minus 1. While the testing of NESTOREv1.0 generally provided reliable results (86% of correct classifications), showing the coherence of the seismic behavior of the Italian clusters, the retrospective test of NESTOREv1.0 led to a failure in forecasting a strong aftershock for the 2018 Molise sequence. In order to understand the differences in the features of seismicity between the 2018 Molise cluster and the other Italian ones, we analyzed in more detail the seismicity, by developing an enhanced template-matching catalog of the area with a low completeness magnitude and applying different methods to identify and characterize clusters in a catalog.

Depending on the method used to identify clusters, one or more clusters resulted, which significantly changed the evaluation of the performances of the forecasting provided by NESTORE. In fact, applying NESTOREv1.0 to the enhanced catalog and assuming that all the Molise seismicity from April to the end of August 2018 belongs to the same cluster, NESTORE classification turns correct (see Sect. 4). However, the main question is if this seismicity belongs to a single cluster or to more than one, generating a discussion on how to select the clusters in such a case. In an ideal scenario with a clear temporal separation, one could distinguish phases more definitively (Lippiello et al. 2019a, 2021; Petrillo et al. 2020). Yet, due to the probabilistic nature of phase overlap, this classification remains inherently uncertain. Molise seismicity can represent, therefore, an ideal case on which to test different analysis techniques of common use as well as less used for cluster analysis (Sect. 5) and others aimed to characterize the geometry and the modalities of the earthquake space–time distribution (Sects. 5 and 6). The analysis with different cluster-identification methods provides different answers on the number of clusters involved. Section 7 is focused on understanding whether the incoherence in results can be due to the presence of fluids.

2 The 2018 Molise increased seismic activity

The study area is located in the Molise region (Southern Italy), at the western boundary of the Adria microplate. It is a complex area, where the extension observed along the Apennine chain is substituted by NW–SE oriented

compression, activating strike-slip mechanisms. The seismicity of the analyzed sequence occurred slightly to the north of the area interested by the Mw 6.0 San Giuliano di Puglia earthquake on 31 October 2002. This major event caused severe damages and casualties and involved right-lateral strike-slip motion, probably due to the reactivation of pre-existing roughly E–W oriented faults (Di Luccio et al. 2005; Chiarabba et al. 2005).

According with the INGV reports and databases (Moretti et al. 2018, 2020) and the reference national catalog ISIDE (ISIDE Working Group 2007), the increased activity of 2018 started with an event of magnitude Mw 4.3 (M_L 4.2) on 25 April 2018, in Montecilfone, close to the town of Campobasso, followed by 34 aftershocks with a Richter M_L magnitude between 0.9 and 2.7 until 9 May. An extremely low seismicity was recorded until August 11. Subsequently, there was a resumption of seismicity with four small events of magnitude M_L between 1.5 and 1.9 between 11 and 14 August, up to the shock of magnitude Mw 4.6 (M_L 4.7) on 14 August, very close in space (less than 2 km) to the event of April 25. This was the strongest event that preceded the Mw 5.1 (M_L 5.2) magnitude earthquake on August 16th. In the time interval between the M_L 4.7 magnitude earthquake and the M_L 5.2 magnitude earthquake, 14 events occurred with M_L between 1.1 and 2.3. In the hours following the strongest shock and up to August 25th, 10 earthquakes with a M_L magnitude greater than 3.0 were recorded, one of which, of magnitude Mw 4.4 (M_L = 4.5), was on the same day as the main event. Table 1 shows the main events occurred, together with their focal mechanism (Moretti et al. 2018, 2020). After the cluster, according to ISIDE catalog (ISIDE Working Group 2007), the seismic activity in the area remained low, with maximum magnitude 3.7 on May 18, 2022, close to Macchia Valfortore village (about 11 km to SSE of the 2002 event and about 30 km to the S of the 2018 cluster), and reactivated some years later on March 28, 2023 close to Montagano village with a moderate earthquake (M_L = 4.6) (about 22 km to the west of 2002 earthquake and 28 km to the SW of 2018 cluster).

Figures 1 and 2 show the evolution in space and time and magnitude of the events in the area obtained by ISIDE catalog. A general SSW migration can be detected (earlier earthquakes—blue dots—are at NNE respect to the later ones—red dots) in Fig. 1a, together with a decrease of depth inside the red rectangle corresponding to the study area (Fig. 1b). Figure 2 shows a marked decrease of seismicity between June and August 2018 (see Fig. 2a between events #1 and #2 of Table 1); a lack of seismicity of magnitude ≥ 2 can be detected also between event #2 and #3 of Table 1 (see Fig. 2b).

In Sect. 3, we present an enhanced template-matching catalog specifically designed for this study. This refined

Table 1 The four main events of the seismicity of Molise in 2018 (close to the village of Montecilfone), and their focal mechanisms (<https://terremoti.ingv.it/>) (see text for details)

#	Date	Time	Lat [deg]	Lon [deg]	Depth [km]	M_L	M_w	Strike [deg]	Dip [deg]	Rake [deg]
1	2018/04/25	09:48:41	41.88	14.86	29	4.2	4.3	256° 347°	88° 80°	170° 2°
2	2018/08/14	21:48:31	41.89	14.84	19	4.7	4.6	104° 14°	88° 83°	-173° -2°
3	2018/08/16	18:19:05	41.87	14.86	20	5.2	5.1	100° 10°	88° 86°	-176° -2°
4	2018/08/16	20:22:34	41.87	14.87	22	4.5	4.4	245° 337°	82° 75°	164° 9°

catalog was developed to better address the unique characteristics of the area under investigation, thereby improving the accuracy and reliability of our analysis.

3 The template-matching catalog

Template-matching seeks earthquakes that strongly resemble well-located events called templates. In this work, template matching is applied to eight months (April–November 2018) of continuous data evaluating 807 earthquakes (the original catalog is from ISIDE (ISIDE Working Group 2007) as templates. We use the template codes (Campanella 2022) rewritten from Vuan et al. (2018) to improve performance and scalability, and to analyze the clustering of the Molise 2018 seismic sequence. The method has been applied to investigate different seismicity patterns in Italy (Sugan et al. 2019, 2023; Vuan et al. 2017, 2020) and in remote regions (Cesca et al. 2022).

The code was applied to daily continuous three-component waveforms covering the time window 1/4/2018–30/11/2018. Seismic data were collected from 29 stations (see Fig. 3), of which 19 were permanent seismic stations of the INGV seismic network (INGV Seismological Data Center 2006), 5 were temporary stations progressively installed by Istituto Nazionale di Geofisica e Vulcanologia (INGV) after the main earthquake of August 16, 2018 (Moretti et al. 2018, 2020), while 5 were accelerometric seismic stations of the Italian Department of the Civil Defense (DPC) (Presidency of Council of Ministers 1972) progressively acquiring in continuous mode since August 20, 2018. We resampled the waveform data to 50 Hz and applied a 3–8 Hz bandpass filter. The templates were trimmed using a 9-s data window starting 4 s before the theoretical S-wave arrival travel time, computed using the ObsPy port (Krischer et al. 2015) of the Java TauP Toolkit routines (Crotwell et al. 1999) and a suitable 1D model (Trionfera et al. 2020). The signal length used in the analysis was determined after a visual inspection of

the complex seismic waveforms that characterized the sequence. We used Kurtosis-based tests to evaluate the signal-to-noise ratio of templates (Baillard et al. 2014) to avoid unwanted signals in the matching technique (Vuan et al. 2018, 2020). A match or detection is a peak above a certain threshold, set at 0.35, in the average of the stacked correlograms. In post-processing, some detections were removed based on the ratio between the average cross-correlation and the noise baseline level, estimated using the daily Median Absolute Deviation (MAD) of the correlograms. It proved to be a robust method for excluding artifacts and false detections. The threshold for this ratio, set after visual inspection of a few examples of detected events, was set at 15 times the MAD. Time windows of 9 s were chosen. Within each window, the template for which the normalized correlation coefficient was the largest used to determine the location and magnitude of the event. In summary, we used restrictive criteria when declaring a positive detection: (a) the average cross-correlation must be greater than or equal to 0.35, (b) it must also be greater than or equal to 15 times MAD, and (c) at least 2 channels must have a cross-correlation greater than or equal to 0.7. Alternatively, we retained as positive detections those with a mean cross-correlation value greater than 0.65 and a threshold ≥ 15 . To improve the robustness of the magnitude assessment, we removed the outliers from the pool of channels used. In the time period analyzed, template-matching helped to detect approximately 4,247 events (Catalog_TM in Electronic Supplement). Figure 4a shows the magnitude distribution of the expanded catalog compared to the original one.

Figure 4b shows the magnitude distribution and the number of events over time. The ability of the templates to find new events varies significantly over time and depends on the availability of stations (stations in the epicentral area are only available after August 16, 2018).

We investigated the completeness magnitude of the catalog by the method of Godano et al. (2024), that is a

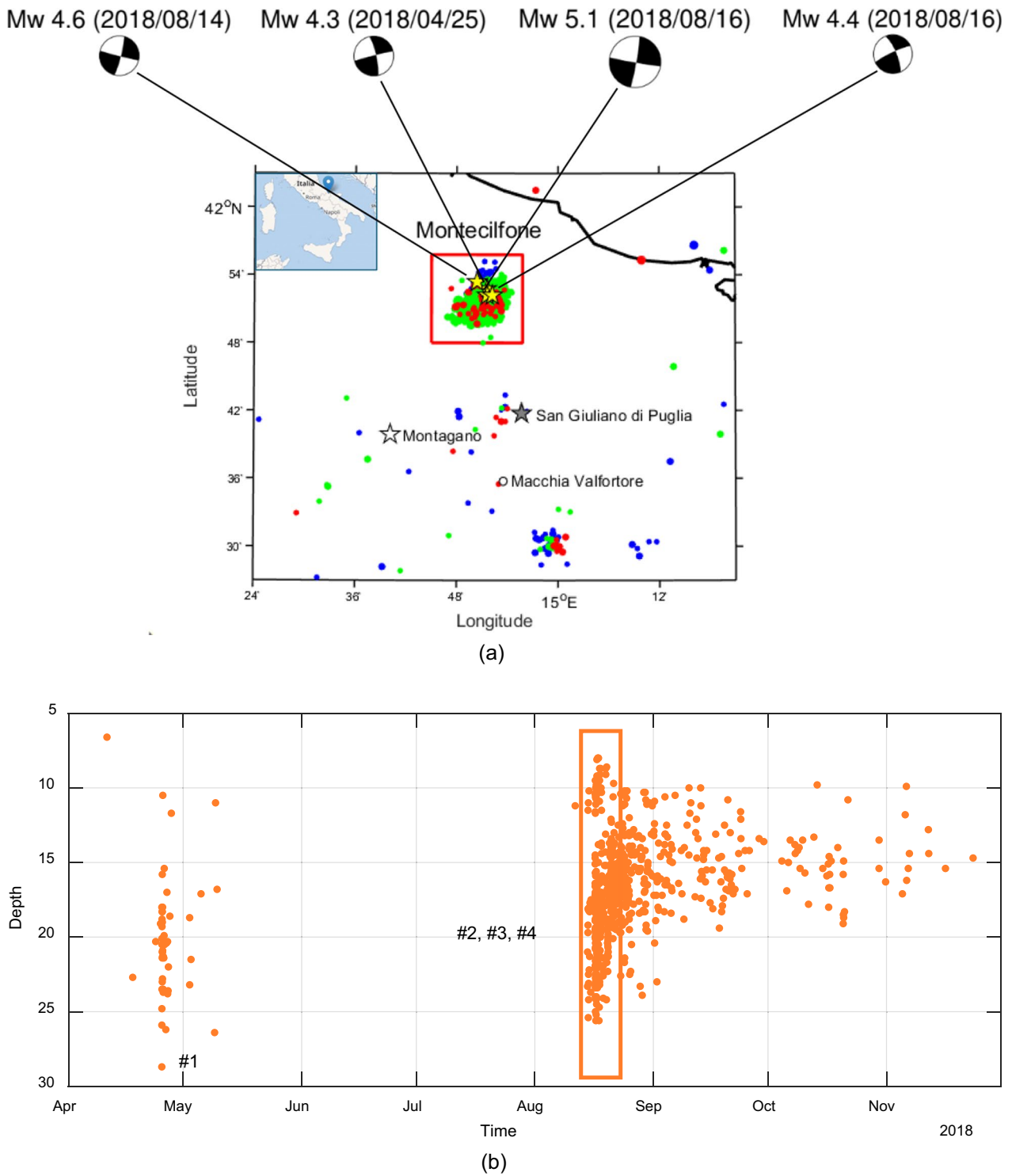
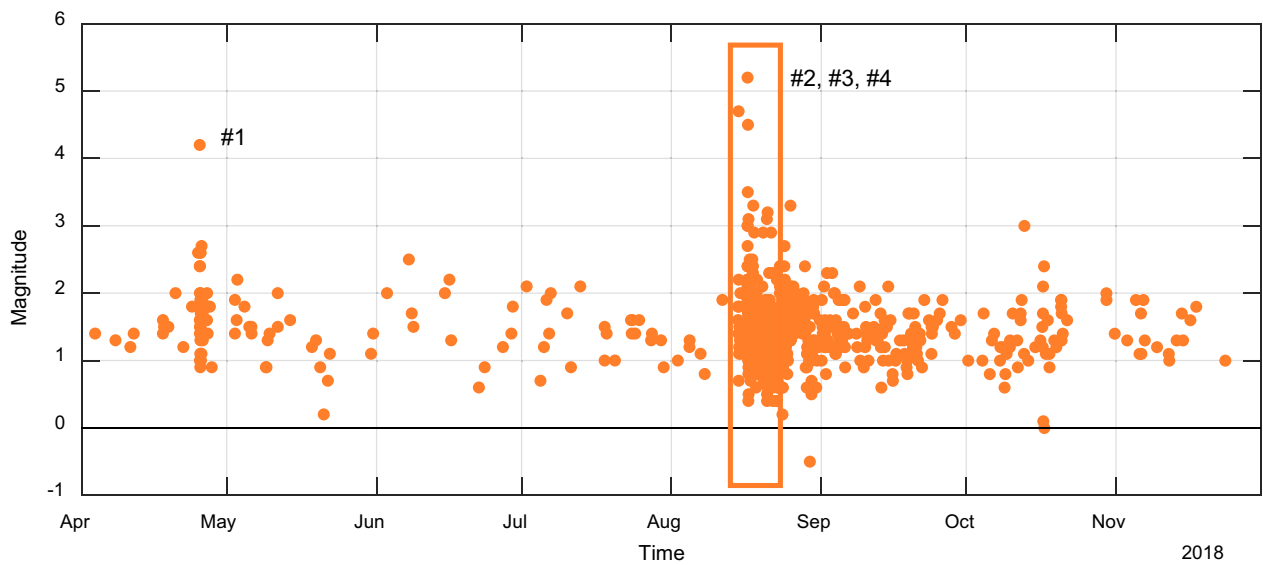
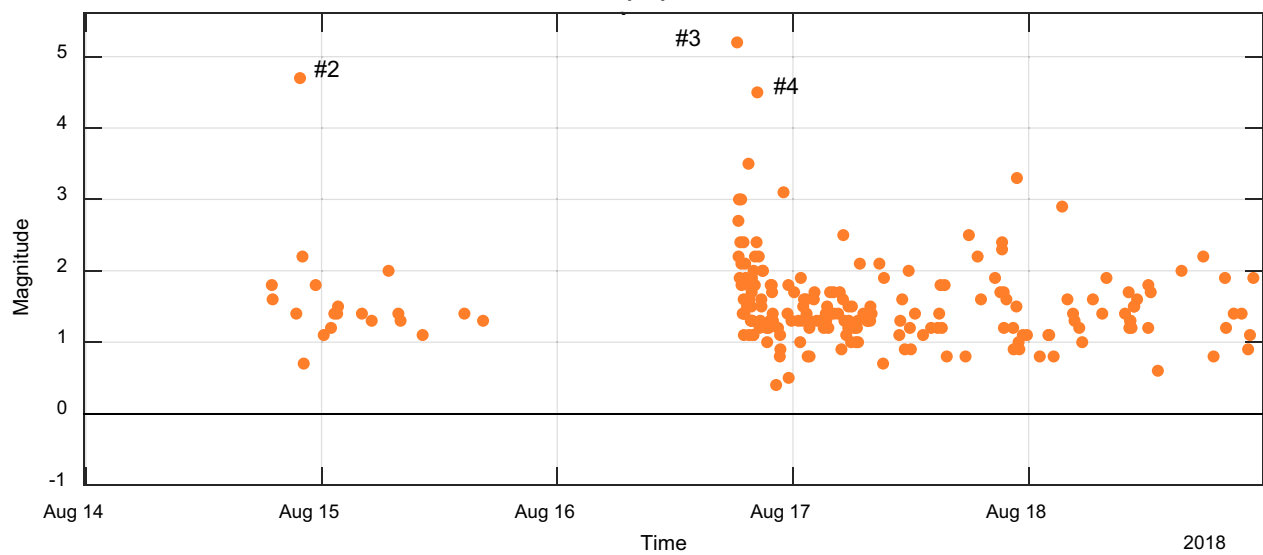


Fig. 1 **a** Evolution in space and time of the events. Black line: coastline. Colored dots: events from April to November 2018. Blue: April–July; green: August–September; red: October–November. White dot: 2022 event. Stars events with magnitude >4: yellow: Montecilfone events of Table 1; gray: San Giuliano di Puglia 2002; white: Montagano 2023. The red square indicates the Montecilfone cluster position in space. Insert: the position of the study area in Italy. The focal mechanisms (beachballs) of the earthquakes listed in Table 1 are shown; the size of the beachballs is proportional to the magnitude. **b** Depth–time plot for the earthquakes inside the red square of (a); orange rectangle shows data on 14–19 August



(a)



(b)

Fig. 2 Magnitude evolution in time for ISIDe catalog: **a** plot of magnitude vs time from April 2018 to December 2018, **b** details on 14–19 August seismicity

generalization of the b-stabilization method from Cao and Gao (2002) (for further results see the Electronic Supplement). The completeness magnitude M_c of the catalog is 1.5 to be compared with that of the original ISIDe catalog for the whole Italy of 2.5 (Gentili and Di Giovambattista 2017; Brondi et al. 2024).

4 Results—NESTORE analysis

The NESTORE algorithm (Gentili and Di Giovambattista 2020) is a machine-learning method that aims to forecast the probability of strong events in a seismicity cluster after a moderate-strong magnitude earthquake (the operative mainshock or o-mainshock). In particular, the algorithm is designed to be applied in the first hours/days after the o-mainshock of magnitude M_m (for Italy $M_m \geq 4$) and forecasts the probability of occurrence of

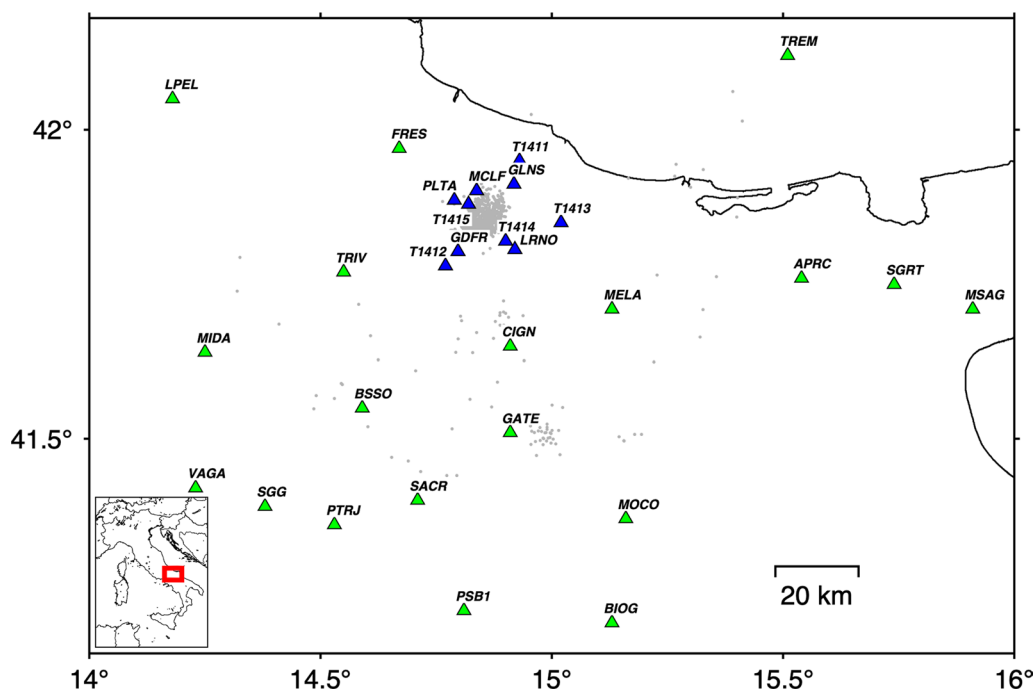


Fig. 3 Map showing the seismic stations used in this study (green triangles: permanent stations active on April 2018; blue triangles: epicentral seismic stations progressively activated in continuous mode from 16 August 2018) and the earthquakes of the ISIDe catalog (807 events in the time window 1/4/2018–31/11/2018), gray dots

an event of magnitude $\geq M_m - 1$. The latest version of the NESTORE algorithm has been implemented in the free software NESTOREv1.0, available on GitHub (Gentili et al. 2023). The software is divided into several independent modules. The default module for identifying clusters is the window-based module, but since the software is modular, other methods for identifying clusters can also be used and replace the window-based module without affecting the rest of the code. NESTORE uses some seismicity features such as the number of earthquakes within the cluster, their energy and their spatial, temporal and magnitude distribution to distinguish between Cluster A (cluster with an aftershock magnitude $\geq M_m - 1$) and Cluster B (the others). Specifically, in the training phase, a 1-node decision tree is trained for each feature to distinguish between the two classes. A threshold is set for each relevant feature, so that most class A training clusters have a feature value above the threshold and most class B clusters have a feature value below the threshold. The procedure is repeated for increasingly longer time intervals after the o-mainshock. After the training procedure, the threshold values are used in the test phase to obtain the classification of the decision trees on an independent dataset. The results obtained from the different features are combined to obtain a final classification based on Bayes' theorem.

Brondi et al. (2023, 2024) applied NESTOREv1.0 to the Italian seismicity (Lolli and Gasperini 2006 and ISIDE catalogs) using the cluster identification method based on predefined windows. They trained it with the seismicity from 1980 to 2009 and tested it with the seismicity from 2010 to 2020. Using this approach, the seismicity of Molise in 2018 was divided into two different clusters, one containing the seismicity from April 2018 ($M_m = 4.2$, corresponding to event #1 in Table 1) to July 2018 and the other containing the seismicity from August onwards ($M_m = 4.7$, corresponding to event #2). The magnitude of completeness in the study area was set at 2.5 for the entire Italian catalog (Gentili and Di Giovambattista 2017). This completeness magnitude is too high to allow an analysis of the first cluster, as NESTORE requires at least a completeness magnitude of $M_m - 2$, i.e., 2.2. Therefore, NESTORE automatically analyzed only the second cluster. For this cluster, it provided erroneous results (Brondi et al. 2023, 2024), as it did not classify it as Type-A (see Table 1).

In this work, the template-matching catalog we developed has a smaller completeness-magnitude. Therefore, we were able to analyze the April seismicity, which yielded some interesting results. Figure 5 shows as circles the values of some seismicity features used by NESTOREv1.0 for all the clusters detected by NESTOREv1.0 on the national territory between 1980

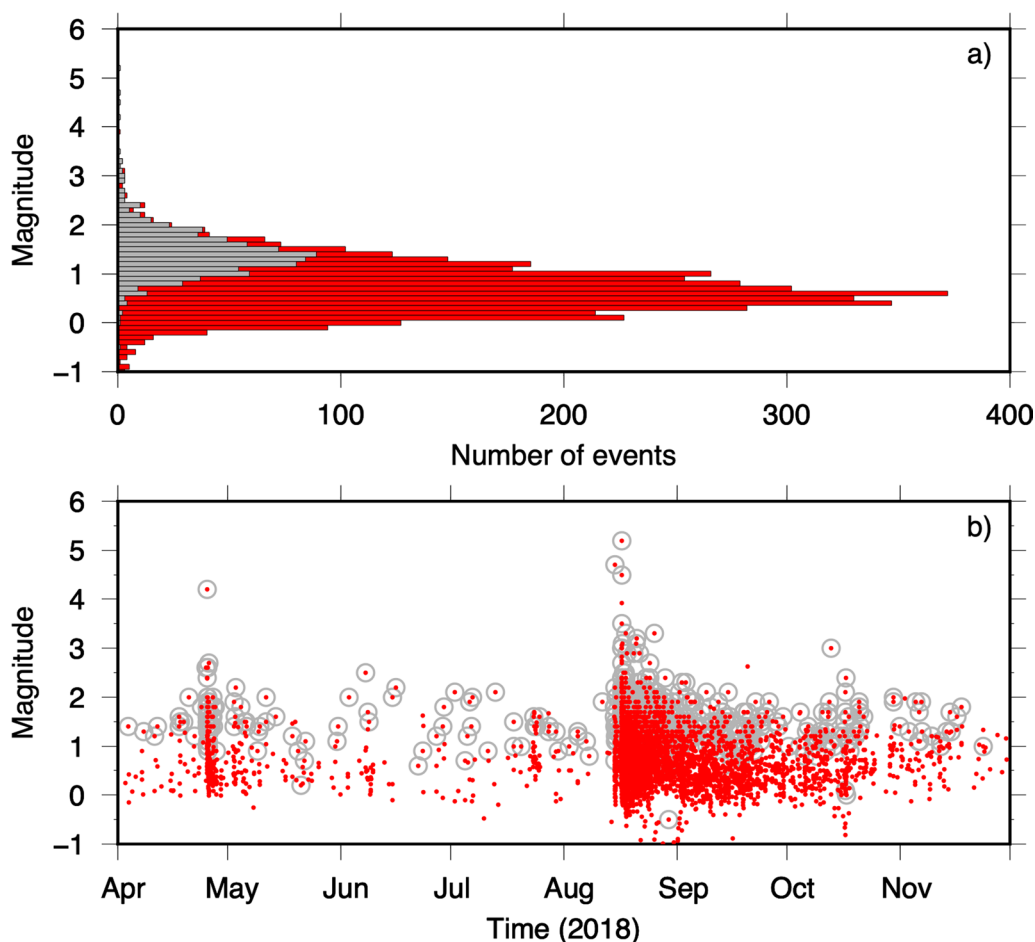


Fig. 4 **a** Histograms showing the magnitude distribution of the augmented catalog (red) compared to the original one (gray). **b** Magnitude distribution over time, colors as in **a**

and 2020, except for Molise, together with the threshold resulting from the training with the whole available dataset (Brondi et al. 2023). In particular, the N_2 , Q , S , and Z features shown in the figure depend on the number, cumulative energy, cumulative source area and spatial distribution of earthquakes in the cluster in the first six hours after the o-mainshock (for more details see Electronic supplement and Gentili et al. 2023). We show Italian Type-A clusters as red circles and Type-B clusters as blue circles. The green star corresponds to the feature values of the April 2018 Molise cluster considered in this work. For all the four features analyzed, the value for the 2018 cluster in Molise is well above the threshold, indicating that the seismicity in Molise for these features is consistent with a type A cluster already 6 h after the o-mainshock. Considering the magnitude 4.2 event that occurred on April 25, 2018 (event # 1 in Table 1) as the o-mainshock, NESTOREv1.0 forecasted the occurrence of the next strong event of magnitude greater than or equal to 3.2 (Type A cluster).

However, there are no events with magnitude greater than or equal to 3.2 in the cluster area between event #1 and July 2018, while in August there are the events #2, #3 and #4, all with a magnitude ≥ 4.5 . The behavior of the 2018 Molise cluster is therefore consistent with the other Italian clusters only if the April and August seismicity belongs to the same cluster or, in other words, the duration of the April cluster is longer than expected by the window-based cluster identification method that successfully identified the other Italian clusters.

5 Results—cluster analysis

In this section, we compare different methods for identifying clusters of seismicity. The first two are the window-based and nearest neighbor methods, the last one is an unconventional method based on fractal dimension. The stochastic declustering method is used to evaluate the probability that the events #1 and #2 belong to the same cluster. Section 5.5 compares different methods results.

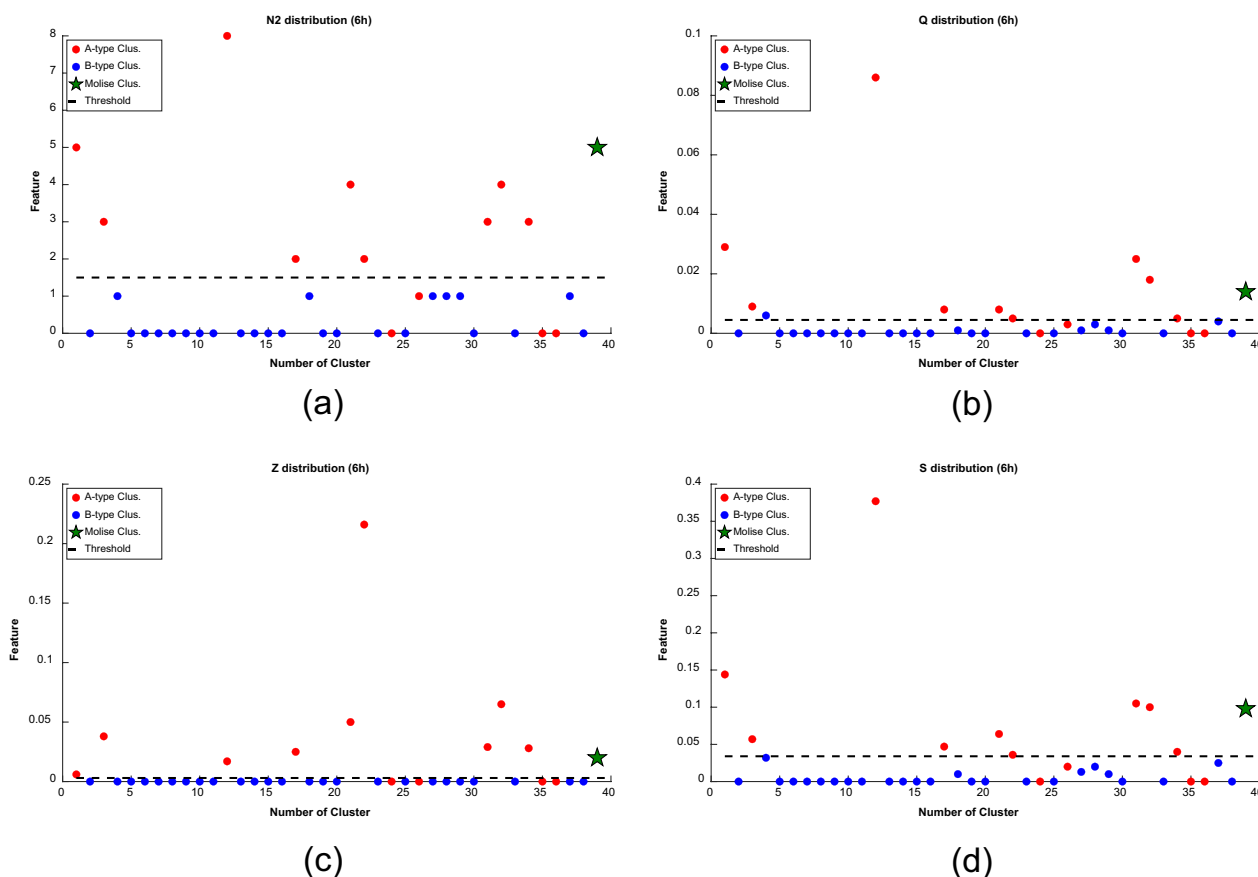


Fig. 5 Molise cluster (green star) compared with other clusters in Italy. **a** N2 feature, **b** Q feature, **c** Z feature, **d** S feature found by NESTOREv1.0 at 6 h after the mainshock. Red circles = A class, blue circles = B class. The black horizontal dotted line indicates the threshold obtained by NESTOREv1.0 training on the 1980–2020 clusters

5.1 Window-based method

One of the simplest methods for defining clusters is to use predefined space- and time-windows. Usually, the area is approximated as a circular area whose radius is a function of the magnitude of the mainshock (van Stiphout et al. 2012). This method has the advantage that it can be quickly applied and does not require information after the mainshock to define the characteristics of the cluster. However, it has the disadvantage that it is only a rough approximation of the extent of the clusters. For example, it is known that clusters characterized by a strike-slip mechanism have an elongated and not circular shape, and selecting a larger circular one would include independent background seismicity into the cluster. Furthermore, the cluster identification process does not recognize the clustered portion of seismicity from the background seismicity within the space and time window. This mainly affects declustered catalogs where "holes" without seismicity are artificially added when this method is used (Gentili

et al. 2017; Peresan and Gentili 2020). In this paper, for the window-based method, in accordance with Gentili and Di Giovambattista (2017), we used the radius R (in km) equation proposed by Uhrhammer (1986) while for T (in days), we adopted the empirical equation of Lolli and Gasperini (2003). By using this method, two clusters are identified, events #1 and #2 belong to different clusters, while events #2, #3 and #4 belong to the same cluster.

5.2 Nearest neighbor method

Among the cluster identification/declustering methods proposed in recent years, the nearest neighbor (NN) approach proved to be successful (Zaliapin et al. 2008; Zaliapin and Ben-Zion 2013; Gentili et al. 2017). This method, based on nearest neighbor distance η of events in the space–time–energy domain (Baiesi and Paczusi 2004), maps the temporal and spatial difference between events in a modified space and time coordinate system. In

particular, the nearest neighbor j of an event i is defined by the metric $\eta_{ij} = t_{ij} r_{ij}^D 10^{-b(m_i)}$, where t_{ij} is the time difference between event i and a following event j , r_{ij} is their epicentral distance, D is the fractal dimension of epicenters, b is the exponent of the Gutenberg–Richter (GR) law and m_i is the magnitude of the first event. Two events form a cluster if the distance $\eta_{ij} < \eta_c$, where η_c is a certain threshold. The distance η_{ij} between any pair of events can be decomposed into a rescaled time, τ_{ij} , and space, s_{ij} for any pair of events. In particular, $\tau_{ij} = t_{ij} 10^{-bm_i/2}$ and $s_{ij} = r_{ij}^D 10^{-bm_i/2}$.

The main advantages of the NN method are that it does not assume a predefined circular space or an end time for the cluster, and does not cause artifacts such as holes in the declustered catalog. However, the disadvantage of this method is that it requires the parameters b , and D as input and it assumes that they are homogeneous within the catalog. Furthermore, clusters that are very close in time and far away in space, or vice versa, may be incorrectly merged because space and time are combined into a single parameter.

In order to estimate the cluster extension, we needed a larger area characterized by background seismicity. Therefore, we analyzed the ISIDE catalog for all earthquakes with longitude $> 14^\circ$ until November 31, 2018 (the date of the end of the Catalog_TM); M_c was set to 2.5 (Gentili and Di Giovambattista 2017). To calculate the fractal dimension D of the spatial distribution of the hypocenters, we used the fixed-size Correlation Integral approach (Mandelbrot 1977; Grassberger 1983), as it is less sensitive to the number of data and shape of the spatial point distribution than other methods (e.g., Bressan

et al. 2016) (see Electronic Supplement), and obtained a value of D of 1.1; b was set to 1 accordingly to Godano and Petrillo (2023) and Godano et al. (2024). Figure 6a, b shows the normalized counts (τ_{ij}, s_{ij}) in a contour plot and the 1D density distribution of η_c respectively. Two different populations can be recognized: the foreshock and aftershock clustering, when $\tau_{ij} s_{ij} < \eta_c$, and the background Poissonian seismicity when $\tau_{ij} s_{ij} > \eta_c$.

By mapping this two-dimensional space into a 1D space (η space), it is possible to determine a threshold to distinguish the clustered from the background seismicity (see Fig. 6a). The value of the threshold can be extracted from the intersection of the fitting curves of the two different populations. According to the procedure, we estimated $\eta_c = 10^{-3.97}$. This method identifies one single cluster to which all the events of Table 1 belong.

5.3 Fractal dimension analysis

To recognize different subclusters, we performed an analysis of the variation with time of the fractal dimension of the spatial shock distribution, by calculating the Correlation Integral on temporal sliding windows of a fixed number of events (see Electronic Supplement).

The analysis was done by using the Catalog_TM in the area (14.75 – 14.93° E 41.80 – 41.93° N) indicated by a red rectangle in Fig. 1. We examined several sliding-window widths to analyze the order of magnitude of the separations between pairs of events, as done by Bressan et al. (2017). We used a time window of 10 events, with the shift of 1 event, since it ensures at least four order of magnitudes of the distances.

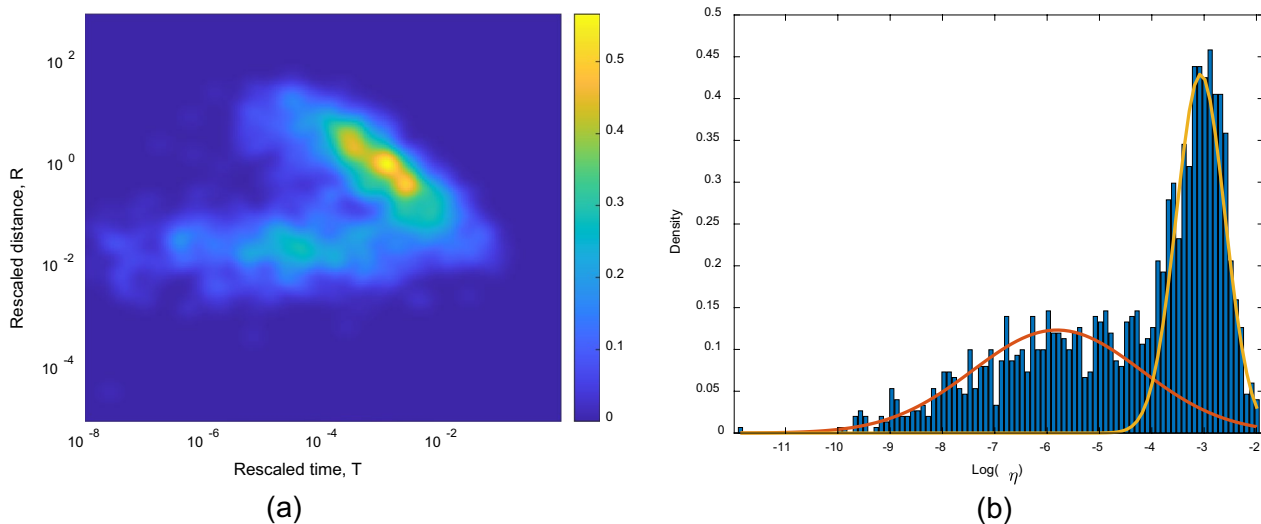


Fig. 6 **a** Bimodal distribution of the normalized time and space coordinates for the 2018 Molise seismicity. The color bar represents the distribution of the density of event pairs. **b** η distribution employed to extract the threshold η_c from the intersection between the fitting curves

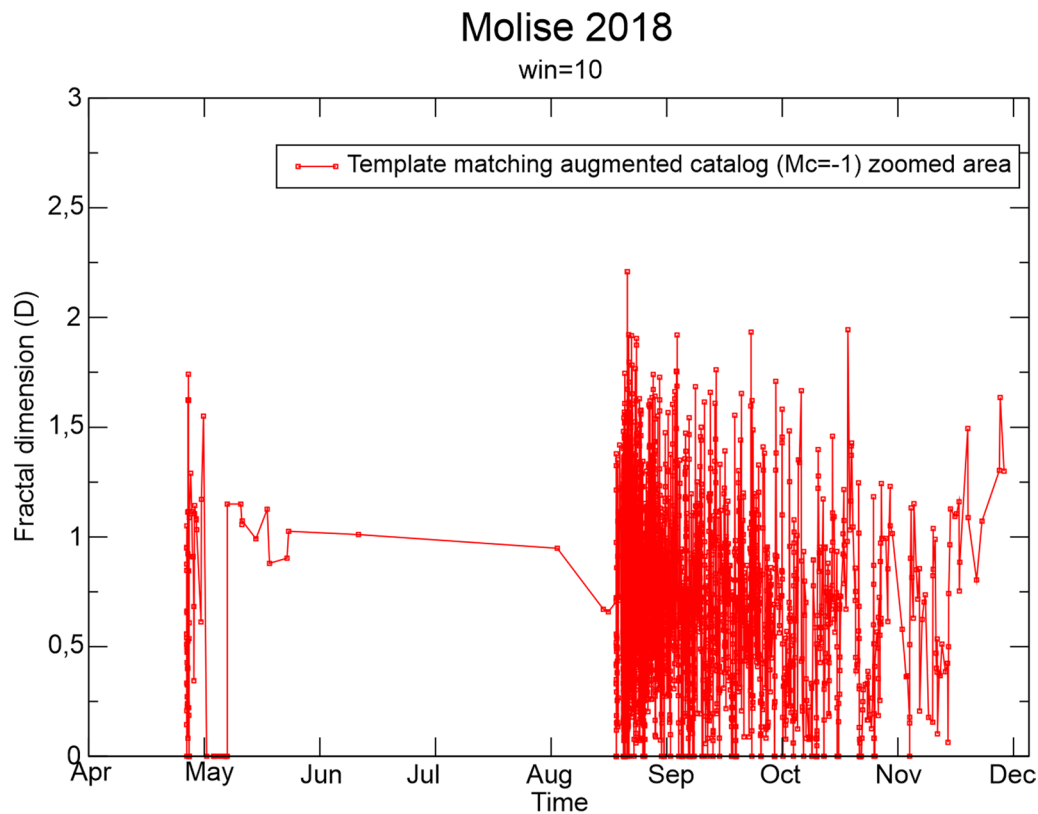


Fig. 7 Fractal dimension of the spatial distribution of the hypocenters obtained by sliding a window of 10 events, with 1 event shift along the augmented catalog, within the area indicated by a red rectangle in Fig. 1

In Fig. 7, the time variation of the fractal dimension so obtained is shown.

The two seismic “crises” of April and August 2018, which followed events # 1 and # 2, are recognizable, marked by high oscillations and reaching the maximum values of D . The values of the fractal dimension decrease after the main shock in April, indicating the end of the first sequence in May. From May to the end of July, an apparent quiescence phase can be recognized, with few earthquakes, and a fractal dimension around 1, indicating a linear propagation. Then, with the events of August, mainly located to the SE of the April ones, the fractal dimension values show clear oscillations, with values oscillating around 1.2 and reaching values close to 2 (planar distribution) three times and 2.2 in one case, indicating the tendency to fill the volume. Values of 1.2 indicate a linear propagation, possibly in depth, being the shocks distributed in this phase along the whole depth interval, from 25 to 8 km. The three main events of August 14 and 16 fall within the same phase, which ended in the first

half of October. The slight increase of the fractal dimension from the mid of October could mark the beginning of a new phase, with the shocks distributed in the same area, but in a depth interval slightly shallower than the preceding phase.

5.4 Stochastic declustering method

Since the choice of parameters in the above declustering models may be subject to biases, it is tempting to ask whether a probabilistic approach is useful in reconstructing the generation tree of the events under consideration. The stochastic declustering proposed by Zhuang et al. (2002) seems to be a suitable candidate for this task.

In order to apply the method, we need to know the conditional intensity function of the ETAS model, which is the summation of contributions from the background seismicity rate and from each of all the previous events (triggering part). Namely, the occurrence rate λ as a function of the history of earthquake occurrence times H_t is:

$$\lambda(H_t) = s(m) \left[\mu(x, y) + \sum_{i:t_i < t} k(m_i)g(t - t_i)f(m_i) \right], \tag{1}$$

where $\mu(x, y)$ is the time-independent space-dependent background rate, $s(m)$ is the probability density function (pdf) of the Gutenberg–Richter law, $k(m_i)$ is the expected number of offsprings from an ancestor of size m_i , $g(t - t_i)$ and $f(m_i)$ are the pdf of the occurrence time and location from an ancestor with magnitude m_i . Since in our study we employ the temporal ETAS model, we neglect the spatial part. In practice, we consider

$$\lambda(t) = \mu + \sum_{i:t_i < t} k(m_i)g(t - t_i) = \mu + K \sum_{i:t_i < t} e^{\alpha(m_i - m_0)}(t - t_i + c)^{-p}, \tag{2}$$

where $\{\alpha, c, p, K, \mu\}$ is the set of parameters to be optimized by means of Maximum Likelihood Estimation (MLE) (Ogata and Zhuang 2006).

Then, it is possible to define two separate subsets of events: background and triggered events. The probability that an event j is a background event is given by:

$$\psi_j = \frac{\mu}{\mu + K \sum_{i:t_i < t_j} e^{\alpha(m_i - m_0)}(t_j - t_i + c)^{-p}}. \tag{3}$$

Conversely, the probability that an event j is triggered by a previous event i is given by:

$$\rho_{ij} = \frac{Ke^{\alpha(m_i - m_0)}(t_j - t_i + c)^{-p}}{\mu + K \sum_{i:t_i < t_j} e^{\alpha(m_i - m_0)}(t_j - t_i + c)^{-p}}. \tag{4}$$

After the matrices ρ_{ij} and ψ_j are obtained, a family tree in the catalog is realized, and it is possible to define the clusters. We would like to underline that the ETAS model employed for the stochastic declustering does not contain clustering magnitude dependence (Petrillo and Zhuang 2022, 2023).

Fitting the ETAS model in the time period 24-04-2018 to 16-08-2018, we obtain $\{\alpha, c, p, K, \mu\}$

$= \{0.5120761, 0.0507983, 1.5737003, 0.0581101, 0.3497437\}$.

With these parameters, the probability that the M_L 4.7 event, which occurred on 14-08-2018, is a direct offspring of the M_L 4.2 event on 24-04-2018 is $\rho_{12} = 0.0284912$, much lower than its background probability $\rho_b = 0.653713497$. The probabilities that this M_L 4.7 event is directly triggered by the M_L 2.0 and M_L 2.2 events, which occurred between the M_L 4.2 and M_L 4.7 events, are 0.00889 and 0.20928, respectively.

The probability that the M_L 4.7 event is triggered by the M_L 2.2 event might be relatively high. However, since the probability that the M_L 2.2 event is triggered by the M_L 4.2 event is of 0.01125, the probability that the M_L 4.2

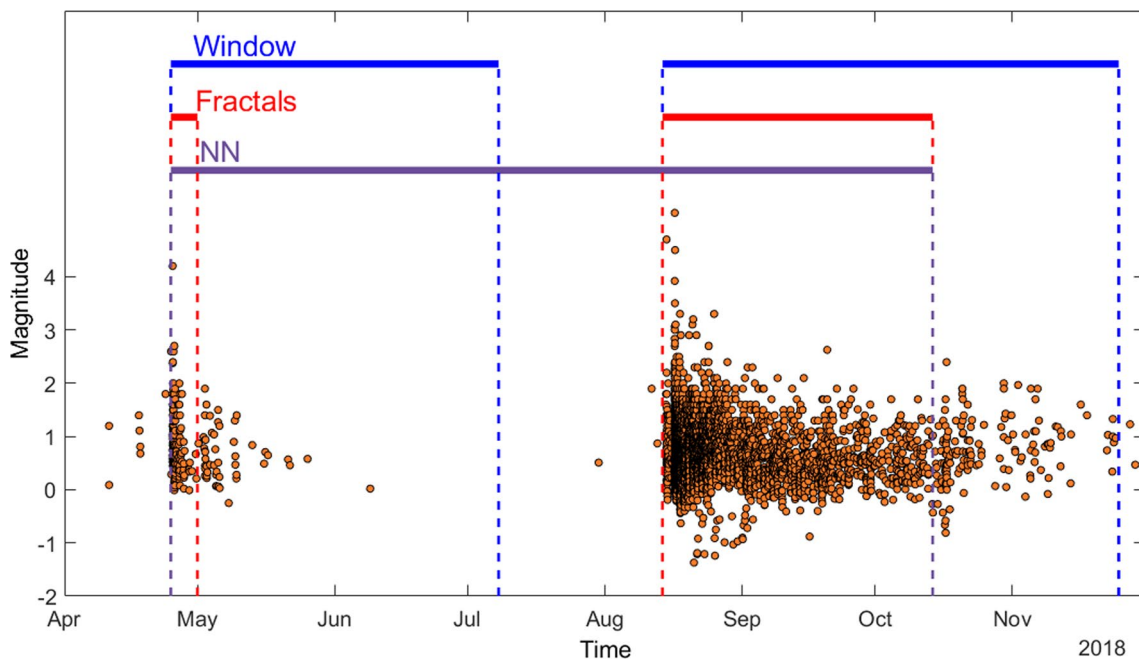


Fig. 8 Comparison among different methods of cluster identification

event indirectly triggers the M_L 4.7 event via the M_L 2.2 event is even lower. Given this probabilistic analysis, and acknowledging the sensitivity of the declustering process to the thresholds values, the M_L 4.7 event is more likely to belong to a different cluster than the M_L 4.2 event. While our results suggest that at least two clusters should be considered, this interpretation depends on the chosen model parameters and thresholds, introducing an element of uncertainty inherent in the stochastic declustering process.

5.5 Cluster methods comparison

Figure 8 shows the temporal comparison of clusters that were determined using different methods. Two methods (window-based and fractal) separate the August seismicity from the April seismicity. This result is probabilistically confirmed by stochastic declustering. In addition, two methods (NN and fractal) further subdivide the mid-October seismicity by separating the August seismicity from the later seismicity.

Due to the ambiguous results, we decided to further analyze the seismic activity.

6 Results—further detailed analysis

In the following session, we further analyze the 2018 Molise seismicity in deeper detail, using the principal component analysis (PCA) and the ETAS algorithm, with the aim to investigate the spatial and temporal features.

6.1 The Principal Component Analysis

Principal Component Analysis (PCA) is a dimension-reduction method that uses the first (centroid) and second moments (variance) of the measured data. The method is used in various fields, as it can find common features from different observations by singular value decomposition of the correlation matrix. As a result, we obtain a concise description of an n -dimensional original data set in the form of m orthogonal functions ($m < n$), accounting for the variance of the data set.

PCA analysis of seismic events can in particular help to reveal certain patterns in the distribution of seismicity and the propagation of ruptures. In particular, we used the multidimensional approach introduced by Rossi and Ebblin (1990) and improved by Bressan et al. (2021). In the construction of the 4D correlation matrix, which can be interpreted as a hyperellipsoid, time is added to the spatial coordinates to also detect temporal changes. All the quantities are normalized, so to have an a -dimensional matrix. The minimum axis of the hyperellipsoid is perpendicular to the plane that best corresponds to the spatial distribution of the hypocenters (Pearson 1901), while the other two spatial axes indicate the extent of

the volume occupied by the aftershocks. The fourth time axis, projected onto space, indicates the direction of propagation of the shocks. We distinguish three main cases:

- The events are mainly contained within the fracturing planes (F);
- The events' distribution indicates the activation of planes, parallel to the first/main one (P);
- The seismic activity tends to migrate, in the direction indicated by the dots (M).

For more details see Bressan et al. (2021).

To be sure to follow the time evolution of the seismic activity, we used sliding windows over which the PCA analysis was performed. We calculated the mean square residual (SR) of the best-fitting plane as a function of the window size, measured in terms of the number of events, to choose the optimal window size (100 events), with the shift of one event.

Figure 9 shows the lower hemisphere stereographic projection of the 4D PCA axes for the Catalog_TM in the region (latitude 41.8–41.93°N; longitude 14.75–14.93°E). The different plots relate to successive periods from April 11, 2018, to November, 23, 2018: in the figures the barycenter of the first and last window used. We can see how the first phase (Fig. 9a), with vertical NE–SW trending planes is followed by the progressive activation of roughly EW-oriented subvertical planes (Fig. 9b, c and e). Until the end of August, in fact, the planes best fitting the shock distribution have NW–SE oriented poles, whereas since September, they rotate to about NS-trending sub-horizontal poles. As said before, the time-axis projections onto space enable to follow the propagation direction of the seismic events. In the first phase (Fig. 9a) we find three main trends: the first is along the fracturing planes (F), indicating mainly the extension in the vertical direction; the second is in a N–S, NNE–SSW direction, indicating a migration of the seismicity in this direction (M). The last is the cluster of points (P) in the plane containing the major and minimum spatial axis, indicating the activation of planes parallel to the main one, upwards. During the sequence (Fig. 9b) containing the main shocks of August 16, the time axis is mainly contained in the fracturing planes, with a prevalence of the vertical direction (F). The other characteristic of this phase is a propagation in E–W direction (M), and again the activation of planes, parallel to the main one (P), that continues also in the time period shown by Fig. 9c (P). This migration is at the origin of the rotation of the planes to E–W subvertical planes (Fig. 9c, e), still alternated to the ENE–WSW trending planes in Fig. 9d, in which the diffusion of the shocks in the fracturing plane (F), and on planes parallel

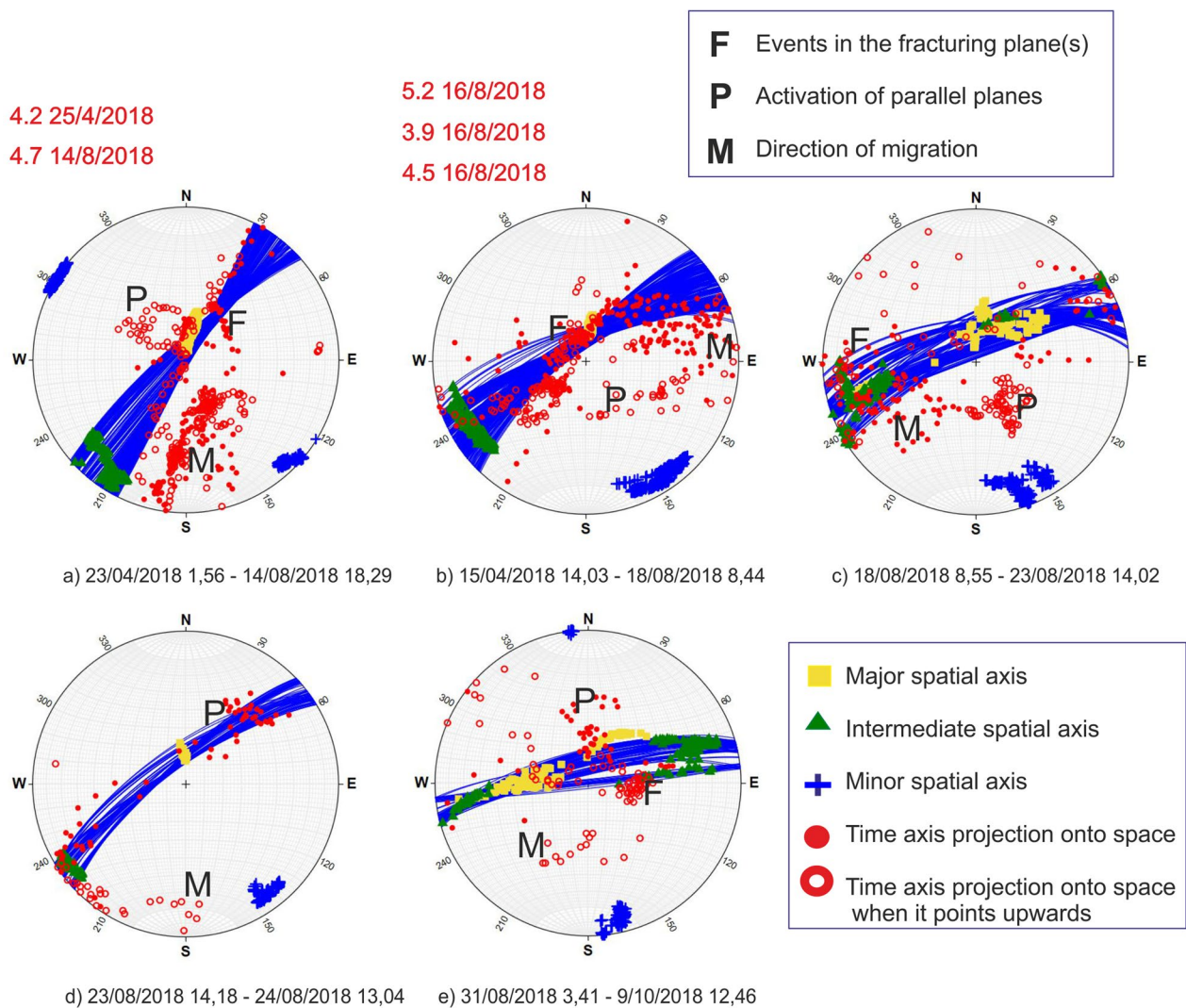


Fig. 9 The lower hemisphere stereographic projection of the 4D PCA axes for the Catalog_{TM} in the region (latitude 41.8–41.93°N; longitude 14.75–14.93°E) from 11-04-2018 to 23-11-2018. At the bottom of each figure, the time barycenter of the first and last ellipsoid considered. Details on the symbols used in the legend and in the text

to it (P), is accompanied by a migration in a direction from NE–SW to N–S, upwards (M). Such migration continues in the last phases of the sequence (Fig. 9e, M).

These results, therefore, would support the hypothesis that the event of April represents the start of a phase of activity, that at the beginning extended mainly in the vertical direction, and then activated with the two main shocks of August, a sheaf of subparallel planes, about EW-oriented. The slight rotation of the plane shown in Fig. 9e could support the hypothesis of the fractal analysis of a new cluster or phase toward the end of the considered time period.

6.2 Relative seismic quiescence detected by the temporal ETAS model

Matsu’ura (1986, 1991) showed that before the onset of a large aftershock, the time series of the transformed time sequence obtained based on the Omori–Utsu formula show lower occurrence rate than the expected standard Poisson process. Such a phenomenon is called "relative" quiescence. This concept has been naturally generalized to the case using this ETAS model as a reference, and is widely used (e.g., Ogata 1988, 1992).

In this section, we only consider the temporal ETAS model with conditional intensity:

$$\lambda(t) = \mu + \sum_{i:t_i < t} Ke^{\alpha(m_i - m_c)} / (t - t_i + c)^p. \quad (5)$$

Given a realization $N = \{t_i : i = 1, 2, \dots, n\}$ of the above point process, the transformation

$$\tau_i = \int_0^{t_i} \lambda(u) du \tag{6}$$

transforms N into a stationary Poisson process with a unit rate (called standard Poisson process). The resulted process $N' = \{\tau_i : i = 1, 2, \dots, n\}$ is called the transformed time sequence. If we replace $\lambda(t)$ by one of its estimates from fitting, $\hat{\lambda}(t)$, which is a reasonable approximation of the true $\lambda(t)$, then the yielded transformed time sequence

should form up approximately a standard Poisson process. If the transformed time sequence deviates from the standard Poisson model, then we can say that the model does not fit the data well. To see whether there are changes in the seismicity patterns, we usually firstly fit the ETAS model to the earthquake data in a certain time interval and then extrapolate the time sequence transformation to earthquake events in other time intervals.

Since the completeness magnitude of the Catalog_{TM} was assessed to be 1.5, in order to be more conservative, we chose 2.0 as the completeness magnitude

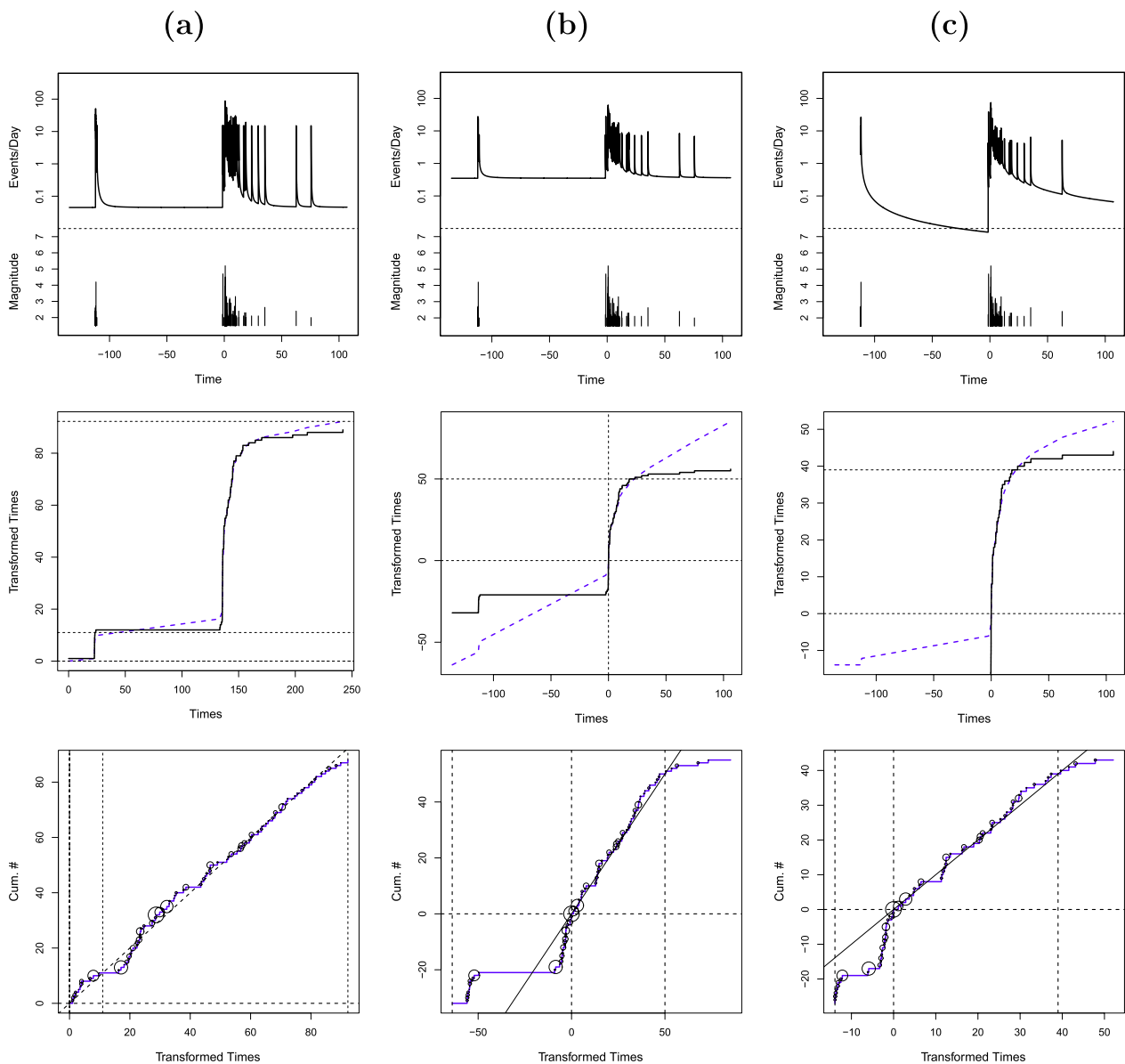


Fig. 10 Fitting results of temporal ETAS model to the 2018 Molise earthquake sequence (time in days) and transformed time sequence analysis. **a** Fitting period: 2018-4-3 to 2018-4-23, test period: 2018-12-1. **b** Fitting period: 2018-8-16.83 to 2018-9-4 test period: 2018-8-23 to 2018-12-1. **c** Fitting period and test period are the same as **b**, but for magnitude $M_L = 2.1$ and above

to ensure that the catalog is complete. We first fitted the ETAS to the M2.0+ earthquake data in the time interval from 3/4/2018 to 28/4/2018 (Fig. 10a) and then extended the transformed time sequence to 1/12/2018 (parameter values: $\mu=0.0448621$, $K=0.0631663$, $\alpha=0.0000000$, $c=0.0557077$, $p=1.8955658$). Here, $\alpha=0$ means that this cluster is more like a swarm than a mainshock–aftershock sequence. The reason for this is: by the definition of the ETAS model, the number of events directly triggered by an earthquake of magnitude m is Poisson distributed with a mean proportional to $\exp[\alpha(m - m_0)]$, and if $\alpha=0$, all the earthquakes have the same number of direct offspring in expectation regardless of their magnitudes. The results show that quiescence occurred between the occurrence times of events #1 and #2 of Table 1 and at the end of the sequence. To confirm the second appearance of the quiescence, we fitted the ETAS model to the time period from the occurrence time of event #3 of Table 1 on 16/8/2018 to 4/9/2018 (Fig. 10b) and extended to calculation of transformed time sequence to 1/12/2018 (parameter values: $\mu=0.3497219$, $K=0.0577392$, $\alpha=0.5313785$, $c=0.0306123$, $p=1.3547957$). The results show that quiescence is clear. The same conclusion can be obtained if we use 2.1 as the magnitude threshold, as shown in Fig. 10c (parameter values: $\mu=0.0000000$, $K=0.0525826$, $\alpha=0.8779779$, $c=0.0137322$, $p=1.0051774$).

In the calculation, we found that the ETAS model with constant background rate is quite unstable, indicating that complicated changes in the stress field might occur during the burst of this earthquake sequence. In some cases, the inadequacy of assuming a stationary background rate in fitting the seismicity has been demonstrated. This could be caused by seismic deviations from ETAS clustering such as fluid up-flow in the fault (Kumazawa and Ogata 2014; Petrillo et al. 2024).

6.3 Fluid diffusion

Like induced seismicity, spontaneous natural seismicity, such as earthquake swarms, sometimes exhibits diffusion-like signatures (e.g., Shapiro and Dinske 2009, and references therein). As a result of fluid intrusion, activity begins at depth and propagates upward over time, giving rise to hypocenters that are distributed over vertical planes and expand over time (Vidale and Shearer 2006).

Most seismic swarms exhibit spatio-temporal migration, whose velocity is used to distinguish between different triggering mechanisms (Vidale and Shearer 2006). Fluid-assisted swarms have typical migration velocities of the order of m/day, whereas aseismic slip-driven swarms generally migrate at faster velocities of

km/h (De Barros et al. 2020, and references therein). The classical method to infer the possible fluid footprint is to analyze the pattern of events' distance in time (t) and space (R) from the known (or hypothesized) fluid origin. In an R - t diagram, the events are distributed on a cloud bounded by a curve that approximates the extent of the rupture zone and describes the distance R_t of the pressure front from the fluid source. The curve has the formula (Shapiro et al. 2002):

$$R_t = \sqrt{4\pi D_h t}, \quad (7)$$

where t is the time from the start of fluid diffusion and D_h is the hydraulic diffusivity. If the diffusion of the fluid stops at a time t_x , the events gradually cease, starting from the zone closest to the origin. A new curve can be defined that separates the two domains “still seismically active” and “already seismically quiet” (Parotidis et al. 2004; Shapiro and Dinske 2009):

$$R_{bf} = \sqrt{2dD_h t \left(\frac{t}{t_x} - 1 \right) \ln \left(\frac{t}{t - t_x} \right)}, \quad (8)$$

where d is 2 if we consider the epicenter position (bidimensional case), and 3 if the vertical information is taken into account and we work in three dimensions.

In addition, fluid injection has recently shown an interplay between fluid pressure and aseismic deformation in triggering and driving seismic activity (De Barros et al. 2020). Various experiments indicated that fluid pressure mainly induces aseismic deformation that triggers seismicity through stress perturbations on fault asperities with appropriate background stresses and frictional instability conditions (De Barros et al. 2020). The alternating bursts of seismicity and quiescence observed in some swarms can be explained by the fault-valve model (Sibson 1992; Rossi et al. 2021). According to Hainzl (2004), at smaller D_h the intervals between subclusters become longer and the total duration of activity increases.

In contrast, the rupture will begin when the fault reaches its critical state (De Barros et al. 2020). Danré et al. (2022), after analyzing several natural and anthropogenic seismic swarms, identified a common driving process: fluid-induced aseismic slip. They also proposed a diagram of velocity versus time duration to distinguish between swarms directly driven by fluid-induced aseismic slip and swarms driven by slow slip (Danré et al. 2022).

We tested the hypothesis that the two activity bursts of April and August 2018 are bound to the same mechanism: a process of fluid diffusion that started with the April event and ended with the seismicity associated with the August shocks and aftershocks. The dominant vertical distribution of events confirmed by the PCA analysis,

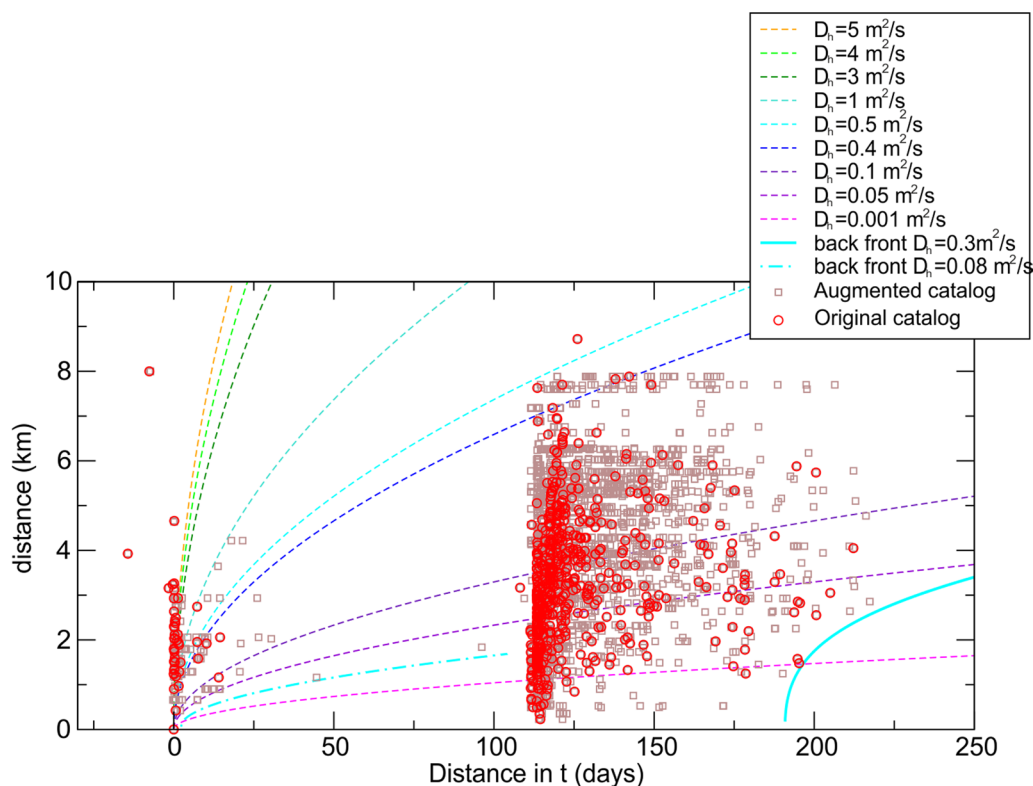


Fig. 11 Distance versus time for the events of the original catalog (red circles) and the Catalog_TM (brown squares). The distances are calculated from the event of April 25, 2018, $M_L = 4.2$. Dashed lines: triggering front for different values of the hydraulic diffusivity D_h (see legend). Fair blue solid and line-dot lines: backfronts (see legend for the diffusivity values)

and the quiescence identified by ETAS suggest fluid diffusion as a possible mechanism.

Therefore, we calculated the distance versus time diagrams for the epicenters of the original catalog and the one augmented by template matching from the main shock of April 25, 2018, and compared the results with the theoretical curves of the triggering front and backfront (Shapiro and Dinske 2009). Figure 11 summarizes the results.

It can be seen that in the first few hours there is a rapid spread of events, reaching a distance of about 3 km within a few hours. Such behavior can be explained with known mechanisms of stress transfer (Toda et al. 2005). In the following month, however, a slower spreading of events (less than 200 m/day) can be observed, which is shown in a curved trajectory in Fig. 11. This becomes even clearer when looking at the data of the catalog_TM. Still, some events of the original catalog also fit into the curves. We calculated different trigger fronts using Eq. (7) of Shapiro et al. (2002) for different values of hydraulic diffusivity, from $5 \text{ m}^2/\text{s}$ to $0.001 \text{ m}^2/\text{s}$. The pattern of events in the diagram of Fig. 11 in the days following the April event is limited in number but fits well with the diffusion hypothesis. In the following days, the activity in the

epicentral area slows down overall, so that we can draw a backfront with $D_h = 0.08 \text{ m}^2/\text{s}$ as a possible value. The activity in August is consistent with a diffusion process, with a triggering front that could have a $D_h = 0.4 \text{ m}^2/\text{s}$. In November, the epicentral area is quiet again, with a backfront with $D_h = 0.3 \text{ m}^2/\text{s}$, showing that permeability has increased as expected during the August–September activity compared to the April activity.

A further analysis was carried out using the approach of Danré et al. (2022). The analysis is based on the mean migration speed. The spatial center of the swarm is identified as the median of the hypocenter coordinates of the first 10 events. The time of the onset is given by the occurrence of the first event, and the seismicity front is determined by evaluating the 90th percentile of the distances of the events from the center of the swarm within a moving window of 50 events. The migration duration is described as the period during which the distance of the front increases steadily (Fig. 12).

In order to obtain a sufficiently large amount of data to calculate the migration velocity, we focused on the seismicity following the event #3. We determined an estimated average migration velocity of $260 \pm 10 \text{ m/day}$ with a duration of 8 days. Figure 13 shows the comparison

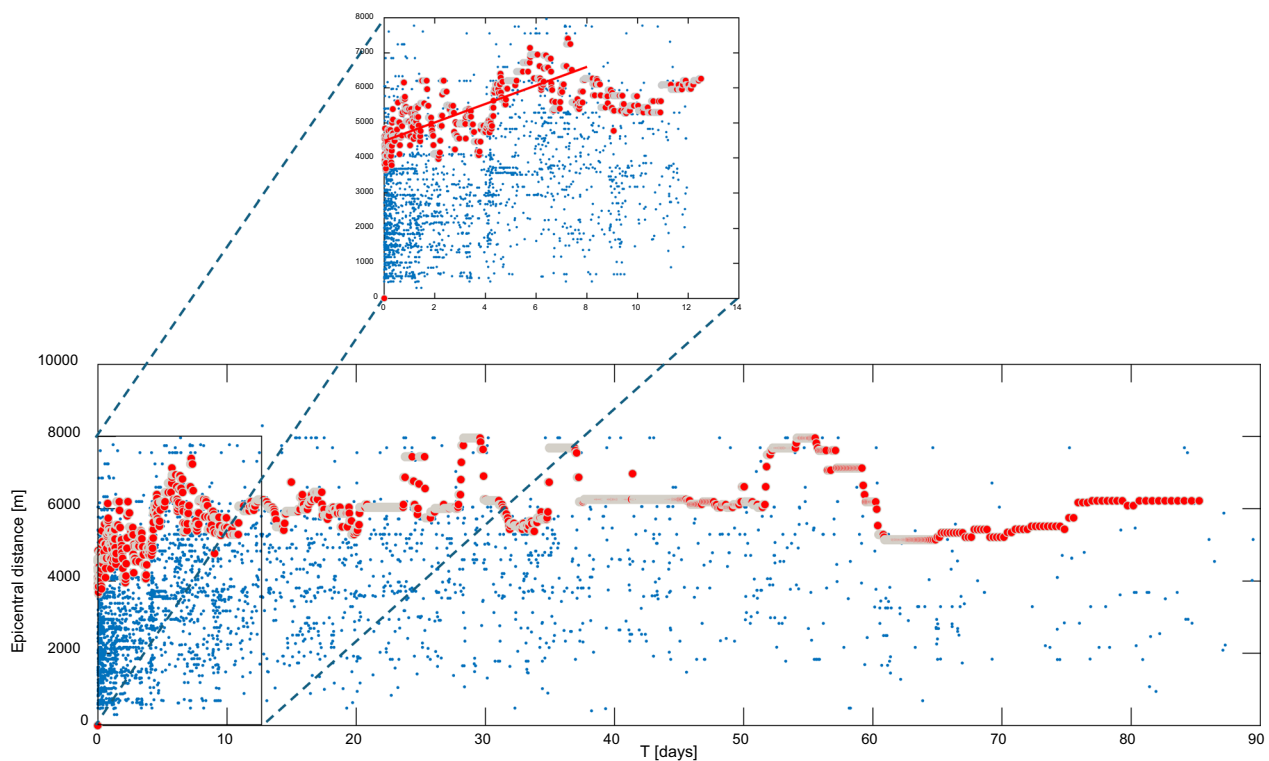


Fig. 12 Seismicity migration after event #3. Blue dots: single earthquake distance from the center of the swarm; red dots: 90th percentile of the distances of the events within a moving window of 50 events. A detail of the first 14 days is shown in the upper part of the figure. Red line: fitting line

between the data in Danré et al. (2022) and the results of this sequence. The data include both the data obtained directly by Danré et al. (2022) and the data they retrieved from the literature. The results of the 2018 Molise sequence are represented by a green star and is compatible with swarms directly driven by fluid-induced aseismic slip (blue symbols).

7 Discussion and conclusions

In this study, we performed a detailed statistical analysis of the seismicity increase in the Molise region in 2018, focusing on the main seismic events in April and August. The sequence was marked by four main earthquakes: the first in April 2018 ($M_L=4.2$) and three additional larger events in August ($M_L=4.7$, $M_L=5.2$, $M_L=4.5$). By applying the NESTORE algorithm, we identified an unusual behavior in the August sequence, where the observed magnitudes exceeded the expected values. This led us to question whether the April and August events were part of the same cluster, a hypothesis that was further investigated using multiple clustering techniques.

Our findings revealed contrasting results depending on the method used. According to the window-based method, the fractal-based approach, and the stochastic

declustering method, the April and August events appeared to belong to different clusters. However, the nearest neighbor method suggested that these events could be part of a single cluster. Additionally, our ETAS model analysis identified two distinct periods of relative quiescence between the main events in April and August, suggesting a potential role of fluid overpressure. These periods of reduced activity could serve as precursors to the subsequent larger earthquakes, including the events of August 14 and 16, and perhaps even the more recent earthquake of March 28, 2023 ($M_L=4.6$).

The results of the principal component analysis suggest that the April event marks the beginning of an active phase, initially manifesting predominantly in a vertical direction, followed by the activation of a series of subparallel planes with the occurrence of the primary shocks in August, oriented roughly east–west. The vertical extension could possibly indicate the presence of fluids (Vidale and Shearer 2006).

Further support for the fluid diffusion hypothesis comes from our distance–time plot analysis, following the methodology of Shapiro and Dinske (2009). We observed a migration of seismicity consistent with fluid-driven processes, with different diffusivity

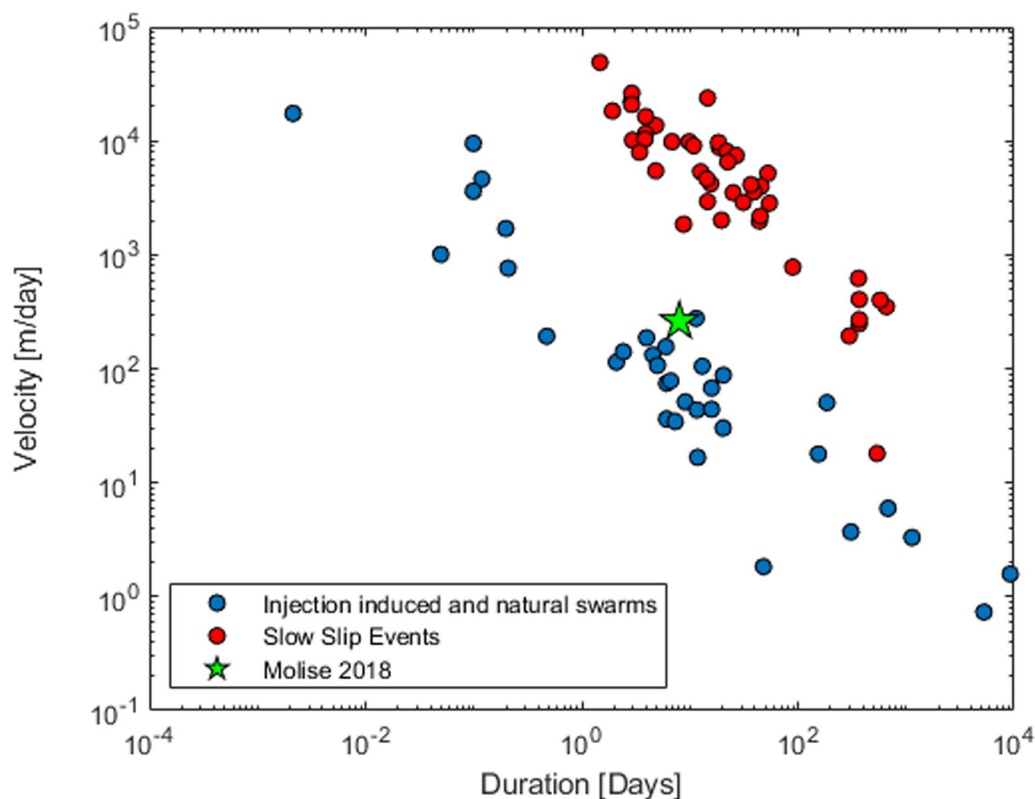


Fig. 13 Velocity versus duration of seismic events migration. Circles: data from Danré et al. (2022). Green star: Molise seismicity migration after event #3

values characterizing the April and August sequences. In particular, the higher diffusivity during the August events suggests an increase in permeability, likely due to the stronger seismic activity in that period. The role of fluids has already been studied in various Italian sequences, demonstrating their role in earthquake migration, source parameters and attenuation of the medium (Di Luccio et al. 2010; Ventura and Giovambattista 2013; Gentili and Gentile 2015; Malagnini et al. 2022; Calderoni et al. 2023). The fact that the diffusivity values we estimated are lower than those reported in other studies (e.g., Di Luccio et al. 2010; Malagnini et al. 2022), but still within the expected range for crustal rocks (Simpson et al. 1988), further supports the role of fluids in this seismic sequence. In particular, they are in agreement with previous observations (Shapiro et al. 2002; Rossi et al. 2018; 2021) and with the values reported by Roeloffs (1996, and references therein) for the kind of rocks that are interested by the sequence (Di Luccio et al. 2005; Patacca and Scandone, 2007; Martino et al. 2020).

Additionally, by employing the methodology of Danré et al. (2022), which distinguishes between swarms driven by fluid-induced aseismic slip and slow slip, we

confirmed fluid migration as a significant factor in the seismicity following the August events.

We also acknowledge the importance of static Coulomb stress transfer as a triggering mechanism for aftershocks (Toda et al. 2005; Console et al. 2006). However, our focus in this study was on exploring whether part of the aftershock sequence could be explained by fluid diffusion. As Wang (2000) pointed out, the Coulomb failure function is influenced by changes in pore fluid pressures, suggesting that fluid migration could complement stress transfer in influencing aftershock behavior. This is further supported by studies such as Piombo et al. (2005), who studied how coseismic stress fields can induce fluid flow, altering Coulomb stress changes and influencing further seismicity.

The periods of relative inactivity observed between the major events in 2018, which we term a "fluid-delayed sequence", could be due to a fault-valve behavior (Sibson 1992; Rossi et al. 2021), with the values of hydraulic diffusivity influencing the intervals between the subclusters and the total duration of the activity (Hainzl 2004),

The deviations we observed from standard statistical models like ETAS, also confirmed by Spassiani et al. (2024) for the part of the cluster starting in August,

indicate that additional physical processes, such as fluid migration, may influence seismicity. These deviations do not necessarily imply that the sequence is anomalous, but rather that it differs from expected statistical norms. Due to the stochastic nature of the ETAS model, the probability that the observed seismicity will occur is low, but not zero. Nevertheless, such different results from cluster identification methods are statistically a rare outcome. Importantly, such deviations have been observed in other contexts, such as in regions with high heat flow (Manganiello et al. 2023), during increased foreshock activity (Petrillo & Lippiello 2021; 2023), fluid triggered seismic activity (Hainzl & Ogata 2005; Kumazawa & Ogata 2014; Petrillo et al. 2024), and so on. Our study reflects the complexity of seismicity and highlights the need for further investigation into such "fluid-delayed sequences" to better understand their role in earthquake triggering.

This work is intended as interesting case study, in which one only cluster is analyzed in deep detail. Such level of detail should not be possible on a large dataset also because for this level of detection accuracy a dedicated template-matching catalog is necessary; not all cluster identification methods proposed here are fully automated and a physical interpretation is necessary. The analyzed seismicity space time distribution, with a long lasting ETAS-detected quiescence between April and August seismicity is not very frequent in Italian seismicity: the results of NESTORE with the window-based method described in Sect. 4 can be a cue to estimate the frequencies of such seismicity in accordance with Brondi et al. (2024). In fact, while the application to the whole of Italy gives good results in 86% of cases, this sequence is among the 14% of cases of misclassification. Changing the cluster definition, the classification is correct.

We would like to discuss why we obtained different results depending on the method chosen to identify clusters. If, as we hypothesize, fluid diffusion is the cause of this behavior, it should be noted that the methods window-based, fractal dimension, NN used in this work only take into account the spatial and temporal evolution of the earthquake location, but not this important physical property. We tested other well-known temporal windows of the window-based methods (van Stiphout et al 2012) to check if the two clusters can be merged by using different laws. In particular, we used the laws by Gardner and Knopoff (1974), the Gruenthal law used in Zmap code (Wiemer 2001), and the time equation proposed by Uhrhammer (1986) but the time distance between events #1 and #2 is too long to merge the clusters. The NN method combines the April and August seismicity into one cluster, probably because in the η -analysis the very small distance between the epicenters of event #1 and #2, which compensates for the large temporal distance. Another

remarkable difference between the methods shown in Fig. 8 is that the end of the August cluster, which is well defined by the NN and fractal analysis that analyze the spatio-temporal distribution of the aftershock data, is missed by the window-based method because in this case the cluster duration is evaluated based on the mainshock magnitude only. Principal component analysis and earthquake migration analysis vice versa can be used to explain this physical behavior.

In conclusion, this study highlights the possible outcomes of model limitation in cluster identification and stresses the necessity for ongoing research into characterizing complex seismic sequences. By improving our capacity to identify and characterize seismic clusters, we can deepen our understanding of seismic activity and enhance our ability to mitigate seismic risk.

Abbreviations

ETAS	Epidemic Type Aftershock Sequence
INGV	Istituto Nazionale di Geofisica e Vulcanologia
ISIDe	Italian Seismological Instrumental and Parametric Database
ISM	The Institute of Statistical Mathematics
NESTORE	NESt TrOnG Related Earthquake
NN	Nearest Neighbor
PCA	Principal Component Analysis
MAD	Median Absolute Deviation
MLE	Maximum Likelihood Estimation
OGS	National Institute of Oceanography and Applied Geophysics - OGS
SSM	Scuola Superiore Meridionale

Supplementary Information

The online version contains supplementary material available at <https://doi.org/10.1186/s40623-024-02096-3>.

Supplementary Material 1.

Supplementary Material 2.

Acknowledgements

Template-matching computations are performed at CINECA in the framework of the HPC-TRES program agreement between OGS and CINECA. Figures were produced using the Generic Mapping Tools (Wessel and Luis 2017) version 6.3.0 (<http://gmt.soest.hawaii.edu>). For Figure 13 we used the free online application Plotdigitizer (<https://plotdigitizer.com/app>) for data extraction. We thank Mario Nicoletti and Luisa Filippi for the data availability of the RAN-DPC accelerometric seismic stations used in this study. We thank Rodolfo Console and two anonymous reviewers for their careful reading of our manuscript and their many insightful comments and suggestions. We wish to thank Rita Di Giovambattista and Alessandro Vuan for their useful suggestions.

Author contributions

Conceptualization, S.G., G.R., G.P.; all authors contributed to methodology, software validation, formal analysis, visualization in the sub-sections they prepared using their personal expertise (in detail: Section 1: G. P., S.G., J.Z., G. R., M. S.; 2: S.G., G.R.; 3: M.S. S.C. 4: S.G., P. B.; 5.1 S.G., P.B.; 5.2 S.G., G.P.; 5.3 G.R.; 5.4 G.P.; 5.5 S.G., P.B.; 6.1 G.R.; 6.2 J. Z.; 6.3 G.R. S. G.; 7 G.R. S.G. G.P., Electronic supplement G. P., G. R. P.B. and Catalog_TM M.S. S.C.; original draft preparation, G. P. and S. G. review and editing, S.G., G. R, P. B., M. S., G. P, J. Z.; supervision, S.G. and J. Z.; project administration, S.G. and J. Z.; funding acquisition, S.G. and J. Z. All authors have read and agreed to the published version of the manuscript.

Funding

Funded by a grant from the Italian Ministry of Foreign Affairs and International Cooperation and Co-funded within the RETURN Extended Partnership and received funding from the European Union Next-Generation EU (National Recovery and Resilience Plan—NRRP, Mission 4, Component 2, Investment 1.3—D.D. 1243 2/8/2022, PE0000005) and by the NEar real-tiME results of Physical and Statistical Seismology for earthquakes observations, modeling and forecasting (NEMESIS) Project (INGV).

Availability of data and materials

The catalog Catalog_TM together with further information on the analysis performed in this paper and are available in the electronic supplements. The code used for template matching is available on Zenodo (<https://doi.org/https://doi.org/10.5281/zenodo.7140418>). The NESTOREv1.0 toolbox is available for free download from GitHub at the address <https://github.com/StefaniaGentili/NESTORE> and the reproducibility package is available on Zenodo <https://zenodo.org/account/settings/github/repository/StefaniaGentili/NESTORE>. Waveform data used in this study are available via EIDA (the European Integrated Data Archive infrastructure within ORFEUS) at <http://www.orfeus-eu.org/webdc3/>. The “Italian Seismological Instrumental and Parametric Data-Base” (ISIDe, ISIDe Working Group 2007) available at <http://iside.rm.ingv.it/iside/> (last accessed on 1 October 2022), and INGV database available at <https://terremoti.ingv.it/> (last accessed on 3 May 2024).

Declarations

Ethics approval and consent to participate

Not applicable.

Consent for publication

Not applicable.

Competing interests

The authors declare no competing interests.

Author details

¹National Institute of Oceanography and Applied Geophysics - OGS, Udine, Italy. ²National Institute of Oceanography and Applied Geophysics - OGS, Trieste, Italy. ³The Institute of Statistical Mathematics, ISM, Tokyo, Japan. ⁴Scuola Superiore Meridionale, SSM, Naples, Italy. ⁵Earth Observatory of Singapore, Nanyang Technological University, Singapore, Singapore.

Received: 17 May 2024 Accepted: 30 October 2024

Published online: 04 December 2024

References

- Anyfadi EA, Gentili S, Brondi P, Vallianatos F (2023) Forecasting strong subsequent earthquakes in Greece with the machine learning algorithm NESTORE. *Entropy* 25:797. <https://doi.org/10.3390/e25050797>
- Baiesi M, Paczuski M (2004) Scale-free networks of earthquakes and aftershocks. *Phys Rev E* 69:066106. <https://doi.org/10.1103/PhysRevE.69.066106>
- Baillard C, Crawford WC, Ballu V, Hibert C, Mangeney A (2014) An automatic kurtosis-based P- and S-phase picker designed for local seismic networks. *Bull Seism Soc Am* 104(1):394–409. <https://doi.org/10.1785/0120120347>
- Bak P, Christensen K, Danon L, Scanlon T (2002) Unified scaling law for earthquakes. *Phys Rev Lett* 88:178501. <https://doi.org/10.1103/PhysRevLett.88.178501>
- Bressan G, Ponton M, Rossi G, Urban S (2016) Spatial organization of seismicity and fracture pattern in NE Italy and W Slovenia. *J Seismol* 20:511–534. <https://doi.org/10.1007/s10950-015-9541-9>
- Bressan G, Barnaba C, Gentili S, Rossi G (2017) Information entropy of earthquake populations in northeastern Italy and western Slovenia. *Phys Earth Planet Inter* 271:29–46. <https://doi.org/10.1016/j.pepi.2017.08.001>
- Bressan G, Barnaba C, Peresan A, Rossi G (2021) Anatomy of seismicity clustering from parametric space-time analysis. *Phys Earth Planet Inter* 320:106787. <https://doi.org/10.1016/j.pepi.2021.106787>
- Brodsky EE, Lay T (2014) Recognizing foreshocks from the 1 April 2014 Chile earthquake. *Science* 344(6185):700–702. <https://doi.org/10.1126/science.1255202>
- Brondi P, Gentili S, Di Giovambattista R (2024) Forecasting strong subsequent events in the Italian territory: a National and Regional application for NESTOREv1.0. *Nat Hazards*. <https://doi.org/10.1007/s11069-024-06913-6>
- Brondi P, Gentili S, Di Giovambattista R (2023) Forecasting strong aftershocks in the Italian territory: A National and Regional application for NESTOREv1.0. *EGU General Assembly 2023, Vienna, Austria*, 23–28 April 2023. 10.5194/egusphere-egu23-5729
- Calderoni G, Improta L (2023) Investigating the role of fluids in the source parameters of the 2013–2014 Mw 5 Matese seismic sequence, Southern Italy. *Seismol Res Lett* 95:299–319. <https://doi.org/10.1785/0220230046>
- Campanella S. (2022) stefanocampanella/EQTM: v0.1.0 (v0.1.0). Zenodo. 10.5281/zenodo.7140418
- Cao A, Gao SS (2002) Temporal variation of seismic b-values beneath north-eastern Japan island arc. *Geophys Res Lett* 29:1334. <https://doi.org/10.1029/2001GL01377>
- Cesca S, Sugan M, Rudzinski Ł, Vajedian S, Niemcz P, Plank S, Petersen G, Deng Z, Rivalta E, Vuan A, Linares MPP, Heimann S, Dham T (2022) Massive earthquake swarm driven by magmatic intrusion at the Bransfield Strait, Antarctica. *Commun Earth Environ* 3:89. <https://doi.org/10.1038/s43247-022-00418-5>
- Chiarabba C, De Gori P, Chiaraluce L, Bordonì P, Cattaneo M, De Martin M, Frepoli A, Michelini A, Monachesi A, Moretti M, Augliera GP, D’Alema E, Frapiccini M, Gassi A, Marzorati S, Di Bartolomeo P, Gentile S, Govoni A, Lovisa L, Romanelli M, Ferretti G, Pasta M, Spallarossa D, Zunino E (2005) Mainshocks and aftershocks of the 2002 Molise seismic sequence, southern Italy. *J Seismol* 9:487–494. <https://doi.org/10.1007/s10950-005-0633-9>
- Console R, Murru M, Catali F (2006) Physical and stochastic models of earthquake clustering. *Tectonophysics* 417:141–153. <https://doi.org/10.1016/j.tecto.2005.05.052>
- Crotwell HP, Owens TJ, Ritsema J (1999) The TauP Toolkit: flexible seismic travel-time and ray-path utilities. *Seismol Res Lett* 70:154–160. <https://doi.org/10.1785/gssrl.70.2.154>
- Danrè P, De Barros L, Cappa F, Ampuero JP (2022) Prevalence of aseismic slip linking fluid injection to natural and anthropogenic seismic swarms. *J Geophys Res Solid Earth*. <https://doi.org/10.1029/2022JB025571>
- De Barros L, Cappa F, Deschamps A, Dublanche P (2020) Imbricated aseismic slip and fluid diffusion drive a seismic swarm in the Corinth Gulf, Greece. *Geophys Res Lett*. <https://doi.org/10.1029/2020GL087142>
- Di Luccio F, Fukuyama E, Pino NA (2005) The 2002 Molise earthquake sequence: What can we learn about the tectonics of southern Italy? *Tectonophysics* 405:141–154. <https://doi.org/10.1016/j.tecto.2005.05.024>
- Di Luccio F, Ventura G, Di Giovambattista R, Piscini A, Cinti FR (2010) Normal faults and thrusts reactivated by deep fluids: the 6 April 2009 Mw 6.3 L’Aquila earthquake, central Italy. *J Geophys Res* 115:B06315. <https://doi.org/10.1029/2009JB007190>
- Gardner JK, Knopoff L (1974) Is the sequence of earthquakes in Southern California, with aftershocks removed, Poissonian? *Bull Seis Soc Am* 64(5):1363–1367
- Gentili S, Di Giovambattista R (2017) Pattern recognition approach to the subsequent event of damaging earthquakes in Italy. *Phys Earth Planet Inter* 266:1–17. <https://doi.org/10.1016/j.pepi.2017.02.011>
- Gentili S, Gentile F (2015) High frequency attenuation k parameter and QS 3D model for south-eastern Alps and north-western Dinarides. *Bollettino Di Geofisica Teorica Ed Applicata* 56:383–406. <https://doi.org/10.4430/bgta0152>
- Gentili S, Di Giovambattista R (2020) Forecasting strong aftershocks in earthquake clusters from northeastern Italy and western Slovenia. *Phys Earth Planet Inter* 303:106483. <https://doi.org/10.1016/j.pepi.2020.106483>
- Gentili S, Di Giovambattista R (2022) Forecasting strong subsequent earthquakes in California clusters by machine learning. *Phys Earth Planet Inter* 327:106879. <https://doi.org/10.1016/j.pepi.2022.106879>
- Gentili S, Di Giovambattista R, Peresan A (2017) Seismic quiescence preceding the 2016 central Italy earthquakes. *Phys Earth Planet Inter* 272:27–33. <https://doi.org/10.1016/j.pepi.2017.09.004>

- Gentili S, Brondi P, Di Giovambattista R (2023) NESTOREv1.0: a MATLAB package for strong forthcoming earthquake forecasting. *Seismol Res Lett* 94(4):2003–2013. <https://doi.org/10.1785/0220220327>
- Godano C, Petrillo G (2023) Estimating the completeness magnitude m_c and the b -values in a snap. *Earth Space Sci*. <https://doi.org/10.1029/2022EA002540>
- Godano C, Petrillo G, Lippiello E (2024) Evaluating the incompleteness magnitude using an unbiased estimate of the b value. *Geophys J Int* 236:994–1001. <https://doi.org/10.1093/gji/ggad466>
- Grassberger P (1983) Generalized dimensions of strange attractors. *Phys Lett* 97A:227–230. [https://doi.org/10.1016/0375-9601\(83\)90753-3](https://doi.org/10.1016/0375-9601(83)90753-3)
- Gutenberg B, Richter CF (1941) Seismicity of the Earth, Geological Society of America, Special Paper No 34. <https://doi.org/10.1130/SPE34-p1>
- Hainzl S (2004) Seismicity patterns of earthquake swarms due to fluid intrusion and stress triggering. *Geophys J Int* 159:1090–1096. <https://doi.org/10.1111/j.1365-246X.2004.02463.x>
- Hainzl S, Fischer T (2002) Indications for a successively triggered rupture growth underlying the 2000 earthquake swarm in Vogtland/NW Bohemia. *J Geophys Res* 107(B12):2338. <https://doi.org/10.1029/2002JB001865>
- Hainzl S, Ogata Y (2005) Detecting fluid signals in seismicity data through statistical earthquake modeling. *J Geophys Res*. <https://doi.org/10.1029/2004JB003247>
- INGV Seismological Data Centre. (2006). Rete Sismica Nazionale (RSN). Istituto Nazionale di Geofisica e Vulcanologia (INGV), Italy. <https://doi.org/10.13127/SD/X0FXNH7QFY>
- ISIDe Working Group (2007) Italian Seismological Instrumental and Parametric Database (ISIDe). Istituto Nazionale Di Geofisica e Vulcanologia (INGV). <https://doi.org/10.13127/ISIDE>
- Kagan YY (1994) Observational evidence for earthquakes as a nonlinear dynamic process. *Physica D* 77:160–192. [https://doi.org/10.1016/0167-2789\(94\)90132-5](https://doi.org/10.1016/0167-2789(94)90132-5)
- Krischer L, Megies T, Barsch R, Beyreuther M, Lecocq T, Caudron C, Wassermann J (2015) ObsPy: A bridge for seismology into the scientific Python ecosystem. *Comput Sci Discov* 8(1):014003. <https://doi.org/10.1088/1749-4699/8/1/014003>
- Kumazawa T, Ogata Y (2014) Nonstationary ETAS models for nonstandard earthquakes. *Ann Appl Stat* 8:1825–1852. <https://doi.org/10.1214/14-AOAS759>
- Lippiello E, Petrillo G, Landes FP, Rosso A (2019a) Fault heterogeneity and the connection between aftershocks and afterslip. *Bull Seismol Soc Am* 109(3):1156–1163. <https://doi.org/10.1785/0120180244>
- Lippiello E, Petrillo G, Godano C, Tramelli A, Papadimitriou E, Karakostas V (2019b) Forecasting of the first hour aftershocks by means of the perceived magnitude. *Nat Commun* 10:2953. <https://doi.org/10.1038/s41467-019-10763-3>
- Lippiello E, Petrillo G, Landes FP, Rosso A (2021) The genesis of aftershocks in spring slider models. *Stat Methods Model Seismogenesis* 1:131–151. <https://doi.org/10.1002/9781119825050.ch5>
- Lolli B, Gasperini P (2003) Aftershocks hazard in Italy Part I: estimation of time–magnitude distribution model parameters and computation of probabilities of occurrence. *J of Seismology* 7:235–257. <https://doi.org/10.1023/A:1023588007122>
- Lolli B, Gasperini P (2006) Comparing different models of aftershock rate decay: the role of catalog incompleteness in the first times after mainshock. *Tectonophysics* 423:43–59. <https://doi.org/10.1016/j.tecto.2006.03.025>
- Malagnini L, Parsons T, Munafò I, Mancini S, Segou M, Geist EL (2022) Crustal permeability changes inferred from seismic attenuation: Impacts on multi-mainshock sequences. *Front Earth Sci* 10:963689. <https://doi.org/10.3389/feart.2022.963689>
- Mandelbrot BB (1977) *Fractals: form, chance, and dimension*. W. H. Freeman & Company, New York. <https://doi.org/10.1007/BF03023043>
- Manganiello E, Herrmann M, Marzocchi W (2023) New physical implications from revisiting foreshock activity in southern California. *Geophys Res Lett*. <https://doi.org/10.1029/2022GL098737>
- Martino S, Antonielli B, Bozzone F, Caprari P, Discenza ME, Esposito C, Fiorucci M, Iannucci R, Marmoni GM, Schilirò L (2020) Landslides triggered after the 16 August 2018 Mw 5.1 Molise earthquake (Italy) by a combination of intense rainfalls and seismic shaking. *Landslides* 17:1177–1190. <https://doi.org/10.1007/s10346-020-01359-w>
- Matsu'ura RS (1986) Precursory quiescence and recovery of aftershock activity before some large aftershocks. *Bull Earthquake Res Inst Univ Tokyo* 61:1–65. <https://doi.org/10.1029/SP032p0008>
- Matsu'ura RS (1991) Case 1: Precursory quiescence and recovery of aftershock activity before some large aftershocks, Evaluation of Proposed Earthquake Precursors (ed. M. Wyss), 8–11, American Geophysical Union, Washington DC, <https://doi.org/10.1029/SP032p0008>
- Mignan A (2014) The debate on the prognostic value of earthquake foreshocks: a meta-analysis. *Sci Rep* 4:4099. <https://doi.org/10.1038/srep04099>
- Mogi K (1963) Some discussions on aftershocks, foreshocks and earthquake swarms: the fracture of a semi-infinite body caused by inner stress origin and its relation to the earthquake phenomena (3rd Paper). *Bull Earthq Res Inst* 41:615–658
- Mogi K (1989) The mechanism of the occurrence of the Matsushiro earthquake swarm in central Japan and its relation to the 1964 Niigata earthquake. *Tectonophysics* 159(1–2):109–119. [https://doi.org/10.1016/0040-1951\(89\)90173-X](https://doi.org/10.1016/0040-1951(89)90173-X)
- Moretti M, De Gori P, Govoni A, Margheriti L, Piccinini D, Pintore S, Valoroso L (2018) Seismic Data acquired by the SISMICO Emergency Group—Molise-Italy 2018–T14. Istituto Nazionale Di Geofisica e Vulcanologia (INGV). <https://doi.org/10.13127/SD/FIR72CHYUW>
- Moretti M, Margheriti L, Govoni A, Marchetti A, Pintore S, Carannante S, D'Alena E, De Gori P, Piccinini D, Valoroso L, Stramondo S (2020) The August 2018 Molise Seismic emergency. SISMICO emergency seismic network deployment and data sharing. *Tech Rep INGV* 418:1–32
- Ogata Y (1988) Statistical models for earthquake occurrences and residual analysis for point processes. *J Am Stat Assoc* 83(401):9–27. <https://doi.org/10.2307/2288914>
- Ogata Y (1992) Detection of precursory seismic quiescence before major earthquakes through a statistical model. *J Geophys Res* 97:19845–19871. <https://doi.org/10.1029/92JB00708>
- Ogata Y, Zhuang J (2006) Space–time etas models and an improved extension. *Tectonophysics* 413(1):13–23. <https://doi.org/10.1016/j.tecto.2005.10.016>
- Omori F (1989) On the aftershocks of earthquakes. *J Coll Sci Imp Univ Tokyo* 7:111
- Parotidis M, Shapiro SA, Rotherth E (2004) Back front of seismicity induced after termination of borehole fluid injection. *Geophys Res Lett*. <https://doi.org/10.1029/2003GL018987>
- Pearson K (1901) On lines and planes of closest fit to systems of points in space. *Phil Mag* 2:559–572. <https://doi.org/10.1080/14786440109462720>
- Peresan A, Gentili S (2020) Identification and characterization of earthquake clusters: a comparative analysis for selected sequences in Italy and adjacent regions. *Bollettino Di Geofisica Teorica Ed Applicata* 61:57–80. <https://doi.org/10.4430/bgta0249>
- Petrillo G, Lippiello E (2021) Testing of the foreshock hypothesis within an epidemic like description of seismicity. *Geophys J Int* 225(2):1236–1257. <https://doi.org/10.1093/gji/ggaa611>
- Petrillo G, Zhuang J (2022) The debate on the earthquake magnitude correlations: a meta-analysis. *Sci Rep* 12:20683. <https://doi.org/10.1038/s41598-022-25276-1>
- Petrillo G, Lippiello E (2023) Incorporating foreshocks in an epidemic-like description of seismic occurrence in Italy. *Applied Science* 13(8):4891. <https://doi.org/10.3390/app13084891>
- Petrillo G, Zhuang J (2023) Verifying the magnitude dependence in earthquake occurrence. *Phys Rev Lett* 131:154101. <https://doi.org/10.1103/PhysRevLett.131.154101>
- Petrillo G, Lippiello E, Landes FP, Rosso A (2020) The influence of the brittle-ductile transition zone on aftershock and foreshock occurrence. *Nat Commun* 11:3010. <https://doi.org/10.1038/s41467-020-16811-7>
- Petrillo G, Kumazawa T, Napolitano F, Capuano P, Zhuang J (2024) Fluids-triggered swarm sequence supported by a nonstationary epidemic-like description of seismicity. *Seismol Res Lett*. <https://doi.org/10.1785/0220240056>
- Piombo A, Martinelli G, Dragoni M (2005) Post-seismic fluid flow and Coulomb stress changes in a poroelastic medium. *Geophys J Int* 162:507–515. <https://doi.org/10.1111/j.1365-246X.2005.02673.x>

- Presidency of Council of Ministers - Civil Protection Department (1972) Italian Strong Motion Network. Int Feder Dig Seismogr Netw. <https://doi.org/10.7914/SN/IT>
- Roeloffs E (1996) Poroelastic techniques in the study of earthquake related hydrologic phenomena. *Adv Geophys* 37:136–195. [https://doi.org/10.1016/S0065-2687\(08\)60270-8](https://doi.org/10.1016/S0065-2687(08)60270-8)
- Rossi G, Ebblin C (1990) Space (3-D) and space-time (4-D) analysis of the aftershock sequences: the Friuli (NE-Italy) case. *Boll Geof Teor Appl* 32(125):37–49
- Rossi G, Fabris P, Zuliani D (2018) Overpressure and fluid diffusion causing non-hydrological transient GNSS displacements. *Pure Appl Geophys* 175:1869–1888. <https://doi.org/10.1007/s00024-017-1712-x>
- Rossi G, Pastorutti A, Nagy I, Braitenberg C, Parolai S (2021) Recurrence of fault-valve behavior in a continental collision area: evidence from tilt/strain measurements in Northern Adria. *Front Earth Sci* 9:641416. <https://doi.org/10.3389/feart.2021.641416>
- Scholz CH (2002) The mechanics of earthquakes and faulting, 2nd edn. Cambridge University Press, Cambridge (10.1017/9781316681473)
- Seif S, Zechar JD, Mignan A, Nandan S, Wiemer S (2019) Foreshocks and their potential deviation from general seismicity. *Bull Seismol Soc Am* 109(1):1–18. <https://doi.org/10.1785/0120170188>
- Shapiro SA, Dinske C (2009) Fluid-induced seismicity: pressure diffusion and hydraulic fracturing. *Geophys Prospect* 2009(57):301–310. <https://doi.org/10.1111/j.1365-2478.2008.00770.x>
- Shapiro SA, Rothert E, Rath V, Rindschwentner J (2002) Characterisation of fluid transport properties of reservoirs using induced microseismicity. *Geophysics* 67:212–220. <https://doi.org/10.1190/1.1451597>
- Sibson RH (1992) Implications of fault-valve behaviour for rupture nucleation and recurrence. *Tectonophysics* 211:283–293. [https://doi.org/10.1016/0040-1951\(92\)90065-E](https://doi.org/10.1016/0040-1951(92)90065-E)
- Simpson DW, Leith WS, Scholz CH (1988) Two types of reservoir-induced seismicity. *Bull Seismol Soc Am* 78:2025–2040. <https://doi.org/10.1785/BSSA0780062025>
- Spassiani I, Gentili S, Console R, Murru M, Taroni M, Falcone G (2024) Reconciling the irreconcilable: window-based versus stochastic declustering algorithms. Submitted to *Geophysical Journal International* [arXiv:2408.16491](https://arxiv.org/abs/2408.16491) [physics.geo-ph] <https://doi.org/10.48550/arXiv.2408.16491>
- Sugan M, Vuan A, Kato A, Massa M, Amati G (2019) Seismic evidence of an early afterslip during the 2012 sequence in Emilia (Italy). *Geophys Res Lett* 46:625–635. <https://doi.org/10.1029/2018GL079617>
- Sugan M, Campanella S, Chiaraluca L, Michele M, Vuan A (2023) The unlocking process leading to the 2016 Central Italy seismic sequence. *Geophys Res Lett* 50:e2022GL101838. <https://doi.org/10.1029/2022GL101838>
- Toda S, Stein RS, Richards-Dinger K, Bozkurt S (2005) Forecasting the evolution of seismicity in southern California: animations built on earthquake stress transfer. *J Geophys Res*. <https://doi.org/10.1029/2004JB003415>
- Trionfera B, Frepoli A, De Luca G, De Gori P, Doglioni C (2020) The 2013–2018 Matese and Beneventano seismic sequences (Central–Southern Apennines): new constraints on the hypocentral depth determination. *Geosciences* 10:17. <https://doi.org/10.3390/geosciences10010017>
- Turcotte D (1997) *Fractals and chaos in geology and geophysics*, 2nd edn. Cambridge University Press, Cambridge (10.1017/CBO9781139174695)
- Uhrhammer R (1986) Characteristics of Northern and Central California seismicity. *Earthquake Notes* 57(1):21
- van Stiphout T, Zhuang J, Marsan D (2012) Seismicity declustering, community online resource for statistical seismicity analysis. <https://doi.org/10.5078/corssa52382934>
- Ventura G, Di Giovambattista R (2013) Fluid pressure, stress field and propagation style of coalescing thrusts from the analysis of the 20 May 2012 M_L 5.9 Emilia earthquake (Northern Apennines, Italy). *Terra Nova* 25:72–78. <https://doi.org/10.1111/ter.12007>
- Vidale JE, Shearer PM (2006) A survey of 71 earthquake bursts across southern California: exploring the role of pore fluid pressure fluctuations and aseismic slip as drivers. *J Geophys Res Solid Earth*. <https://doi.org/10.1029/2005JB004034>
- Vuan A, Sugan M, Chiaraluca L, Di Stefano R (2017) Loading rate variations along a midcrustal shear zone preceding the Mw 6.0 earthquake of 24 August 2016 in Central Italy. *Geophys Res Lett* 44:12, 170–12, 180. <https://doi.org/10.1002/2017GL076223>
- Vuan A, Sugan M, Amati G, Kato A (2018) Improving the detection of low-magnitude seismicity preceding the Mw 6.3 L'Aquila earthquake: development of a scalable code based on the cross-correlation of template earthquakes. *Bull Seism Soc Am*. 108(1):471–480. <https://doi.org/10.1785/0120170106>
- Vuan A, Brondi P, Sugan M, Chiaraluca L, Di Stefano R, Michele M (2020) Intermittent slip along the Alto Tiberina low-angle normal fault in central Italy. *Geophys Res Lett*. <https://doi.org/10.1029/2020GL089039>
- Wang H (2000) *Theory of linear poroelasticity with applications to geomechanics and hydrogeology*. Princeton University Press, Princeton
- Wessel P, Luis JF (2017) The GMT/MATLAB toolbox. *Geochem Geophys Geosyst* 18:811–823. <https://doi.org/10.1002/2016GC006723>
- Wiemer S (2001) A software package to analyze seismicity: ZMAP. *Seismol Res Lett* 72:374–383. <https://doi.org/10.1785/gssrl.72.3.373>
- Zaliapin I, Ben-Zion Y (2013) Earthquake clusters in southern California I: identification and stability. *J Geophys Res Solid Earth* 118:2847–2864. <https://doi.org/10.1002/jgrb.50179>
- Zaliapin I, Gabrielov A, Keilis-Borok V, Wong H (2008) Clustering analysis of seismicity and aftershock identification. *Phys Rev Lett* 101:018501. <https://doi.org/10.1103/PhysRevLett.101.018501>
- Zhuang J, Ogata Y, Vere-Jones D (2002) Stochastic declustering of space-time earthquake occurrences. *J Am Stat Assoc*. <https://doi.org/10.1198/016214502760046925>

Publisher's Note

Springer Nature remains neutral with regard to jurisdictional claims in published maps and institutional affiliations.